RESEARCH ARTICLE

Inhibiting the Mammalian Target of Rapamycin Blocks the Development of Experimental Cerebral Malaria

Emile B. Gordon,[a]* Geoffrey T. Hart,[a] Tuan M. Tran,[a] Michael Waisberg,[a]* Munir Akkaya,[a] Jeff Skinner,[a] Severin Zinöcker,[a]* Mirna Pena,[a] Takele Yazew,[a] Chen-Feng Qi,[a] Louis H. Miller,[b] Susan K. Pierce[a]

Laboratory of Immunogenetics[a] and Laboratory of Malaria and Vector Research,[b] National Institute of Allergy and Infectious Diseases, National Institutes of Health, Rockville, Maryland, USA

* Present address: Emile B. Gordon, Perelman School of Medicine, University of Pennsylvania, Philadelphia, Pennsylvania, USA; Michael Waisberg, Department of Pathology, University of Virginia School of Medicine, Charlottesville, Virginia, USA; Severin Zinöcker, AbbVie Norway, Fornebu, Norway.

E.B.G., G.T.H., and T.M.T. contributed equally to this work.

ABSTRACT **Malaria is an infectious disease caused by parasites of several *Plasmodium* spp. Cerebral malaria (CM) is a common form of severe malaria resulting in nearly 700,000 deaths each year in Africa alone. At present, there is no adjunctive therapy for CM. Although the mechanisms underlying the pathogenesis of CM are incompletely understood, it is likely that both intrinsic features of the parasite and the human host's immune response contribute to disease. The kinase mammalian target of rapamycin (mTOR) is a central regulator of immune responses, and drugs that inhibit the mTOR pathway have been shown to be antiparasitic. In a mouse model of CM, experimental CM (ECM), we show that the mTOR inhibitor rapamycin protects against ECM when administered within the first 4 days of infection. Treatment with rapamycin increased survival, blocked breakdown of the blood-brain barrier and brain hemorrhaging, decreased the influx of both $CD4^+$ and $CD8^+$ T cells into the brain and the accumulation of parasitized red blood cells in the brain. Rapamycin induced marked transcriptional changes in the brains of infected mice, and analysis of transcription profiles predicted that rapamycin blocked leukocyte trafficking to and proliferation in the brain. Remarkably, animals were protected against ECM even though rapamycin treatment significantly increased the inflammatory response induced by infection in both the brain and spleen. These results open a new avenue for the development of highly selective adjunctive therapies for CM by targeting pathways that regulate host and parasite metabolism.**

IMPORTANCE **Malaria is a highly prevalent infectious disease caused by parasites of several *Plasmodium* spp. Malaria is usually uncomplicated and resolves with time; however, in about 1% of cases, almost exclusively among young children, malaria becomes severe and life threatening, resulting in nearly 700,000 deaths each year in Africa alone. Among the most severe complications of *Plasmodium falciparum* infection is cerebral malaria with a fatality rate of 15 to 20%, despite treatment with antimalarial drugs. Cerebral malaria takes a second toll on African children, leaving survivors at high risk of debilitating neurological defects. At present, we have no effective adjunctive therapies for cerebral malaria, and developing such therapies would have a large impact on saving young lives in Africa. Here we report results that open a new avenue for the development of highly selective adjunctive therapies for cerebral malaria by targeting pathways that regulate host and parasite metabolism.**

Received 28 April 2015 **Accepted** 1 May 2015 **Published** 2 June 2015

Citation Gordon EB, Hart GT, Tran TM, Waisberg M, Akkaya M, Skinner J, Zinöcker S, Pena M, Yazew T, Qi C-F, Miller LH, Pierce SK. 2015. Inhibiting the mammalian target of rapamycin blocks the development of experimental cerebral malaria. mBio 6(3):e00725-15. doi:10.1128/mBio.00725-15.

Editor L. David Sibley, Washington University School of Medicine

Address correspondence to Susan K. Pierce, spierce@nih.gov.

This article is a direct contribution from a Fellow of the American Academy of Microbiology.

Malaria is a highly prevalent infectious disease caused by parasites of several *Plasmodium* spp., the most deadly of which, *Plasmodium falciparum*, prevails in Africa. In individuals living in areas where malaria is endemic, it is usually uncomplicated and resolves with time even in the absence of treatment with antimalarial drugs. However, in about 1% of cases, almost exclusively among young children, malaria becomes severe and life threatening, resulting in nearly 700,000 deaths each year in Africa alone (1). Among the most severe complications of *P. falciparum* infection in humans is human cerebral malaria (HCM) with a case fatality rate of 15 to 20% in African children despite effective antimalarial chemotherapy (2, 3). HCM takes a second toll on African children, leaving survivors at high risk of debilitating neurological defects (4). At present, we have no effective adjunctive therapies for HCM, and developing such therapies in combination with antimalarial drugs would have a large impact on improving global public health.

Currently, our understanding of the pathogenesis of HCM is far from complete and relies heavily on the analysis of histopathology of brain tissue from children who died from HCM (5, 6). Although HCM is a clinically heterogeneous disease, the commonly accepted definition of HCM centers around neurological

symptoms, ultimately unarousable coma, with the presence of infected red blood cells (iRBCs) in the peripheral circulation system with no other apparent causes of coma (7). Recently, the correct diagnosis of HCM was greatly improved by the use of retinal exams to identify histological features of HCM, correcting what was estimated to be 25 to 30% misdiagnosed cases (8). Sequestration of iRBCs on the brain vascular endothelium is a defining feature of HCM (5). Other common features of the brain histopathology in clinically well-characterized HCM patients include brain microhemorrhages associated with axonal and myelin damage, disruption of the blood-brain barrier (BBB), and brain swelling (5, 6). Systemic activation of the endothelium has also been reported in HCM patients and appears to correlate with disease severity (9). HCM is also characterized by the production of high levels of proinflammatory cytokines and chemokines that have been correlated with HCM pathogenesis (10, 11). The accumulation of both monocytes with phagocytosed hemozoin (5) and platelets (12), as well as a small number of intravascular leukocytes, including $CD8^+$ T cells, has also been observed in brain sections of HCM patients (5, 12). As both the host immune response and sequestration of iRBCs appear to contribute to the pathogenesis of HCM, successful therapies may be ones that target both the host immune response and the parasite.

The mouse model of CM, experimental CM (ECM), recapitulates many characteristics of HCM and therefore may be a useful tool to identify candidates for adjunctive therapy in the human disease (13, 14). Infection of susceptible C57BL/6 mice with *Plasmodium berghei* ANKA (*Pb*A) parasites results in death of up to 100% of mice usually within 6 to 14 days postinfection (p.i.) following clear signs of neurological damage, including paralysis, ataxia, convulsions, and coma (13). Strains of mice resistant to *Pb*A-induced ECM do not show clinical signs of neurological damage but die 2 to 3 weeks after infection due to anemia caused by hyperparasitemia (13). Examination of the brains of mice with late-stage ECM show many of the features common to HCM, including accumulation of iRBCs along venular endothelium, microhemorrhages, breakdown of the BBB, and brain swelling (7, 13). Although the degree of sequestration of iRBCs in the brains in ECM appears in general to be less than that in HCM (14), the presence of iRBCs in the brains of infected mice has been shown to be necessary for the development of ECM (15–17). ECM is also associated with a marked accumulation of various immune cells in the brains of infected animals, including T cells, monocytes, neutrophils, and NK cells. In particular, recent data provided evidence that the accumulation of $CD8^+$ T cells in the brains of infected animals and their production of granzyme B and perforin are required for the development of ECM (15, 18, 19). In 2013, Howland et al. (20) provided evidence that parasite-specific $CD8^+$ T cells interact with parasite antigens cross-presented on major histocompatibility complex (MHC) class I molecules on the brain endothelium in ECM. Recently, Pai et al. (21) used two-photon intravital microscopy to visualize leukocyte behavior in the brains of *Pb*A-infected mice during ECM. They showed that monocytes accumulated in the brain 1 or 2 days prior to the onset of neurological symptoms and showed decreased rolling speeds due to activation of the endothelium as disease severity increased. Adoptive transfer experiments showed that the behavior of monocytes was dependent on the recruitment of $CD8^+$ T cells to the brain. Proinflammatory cytokines also appear to play a critical role in ECM, particularly gamma interferon (IFN-γ), tumor necrosis factor (TNF), and lymphotoxin α (7). Indeed, it was possible to induce ECM in ECM-resistant BALB/c mice by inducing proinflammatory cytokines by treatment with the Toll-like receptor agonist, CpG, during *Pb*A infections (22). Taken together, these results support a model for the pathogenesis of ECM in which infection induces inflammatory cytokines that activate endothelial cells to process and present antigens from iRBCs that accumulated on the activated brain endothelium via MHC class I molecules, marking these cells as targets of parasite-specific $CD8^+$ T cells (23).

The evolutionarily conserved serine/threonine kinase mammalian target of rapamycin (mTOR) plays a central role in regulating the outcome of antigen recognition in the adaptive immune system (24). mTOR functions at a central node of several evolutionarily conserved pathways that regulate stress responses, metabolism, autophagy, and survival. By integrating these pathways with immune cell receptor signaling pathways, mTOR serves to regulate immune responses (25). Targeting mTOR by rapamycin is proving to be an effective means of suppressing immune responses primarily due to the ability of rapamycin to inhibit effector T cell differentiation and promote regulatory T cell (Treg) differentiation (25). In addition, rapamycin has been shown to inhibit parasite growth *in vitro* through its interaction with the single *Plasmodium falciparum* FK506 binding protein *Pf*FKBP35, and consequently, *Pf*FKBP35 is considered a promising target for antimalarial drugs (reviewed in reference 26). Although *Plasmodium* parasite genes do not encode an mTOR homolog, the mTOR ATP-competitive kinase inhibitors, Torins, have been recently shown to inhibit parasite growth (27), possibly through their inhibition of parasite phosphoinositide 3 kinases that are members of the mTOR family.

Here we provide evidence that rapamycin treatment administered as late as 4 days p.i. protects mice from ECM. The most striking effect of rapamycin on disease progression was the prevention of the breakdown of the BBB and brain hemorrhaging and the reduction in the numbers of T cells and iRBCs that accumulate in the brain. Rapamycin markedly altered transcriptional profiles in the brains of infected mice, and analysis of these transcriptional changes predicted that rapamycin inhibited leukocyte trafficking to and proliferation in the brain. Remarkably, rapamycin treatment is protective against ECM, despite significantly increasing immune inflammation both peripherally and in the brain. Rapamycin's effect on parasite growth is complex *in vivo*, functioning to elevate peripheral parasitemia and decrease parasite loads in the brain. Recent studies suggest that several additional metabolic pathways that are activated in T cells following antigen recognition are also required to direct the resulting response (25). The results presented here open a new avenue for the development of adjunctive therapies for HCM by targeting metabolic pathways that regulate immune responses and possibly parasite growth.

RESULTS

Rapamycin treatment protects against ECM. To determine the effect of rapamycin on the development of ECM, C57BL/6 mice were infected with *Pb*A and injected intraperitoneally with a vehicle control solution or with rapamycin (1.0 mg/kg of body weight) daily starting 1, 4, or 5 days p.i. All vehicle-treated mice developed severe neurological symptoms by day 6 p.i. and either died or were euthanized by day 9 p.i. (Fig. 1A). In contrast, mice that began daily rapamycin treatment on either day 1 or 4 p.i. did not develop symptoms of ECM and survived longer than untreated mice. Be-

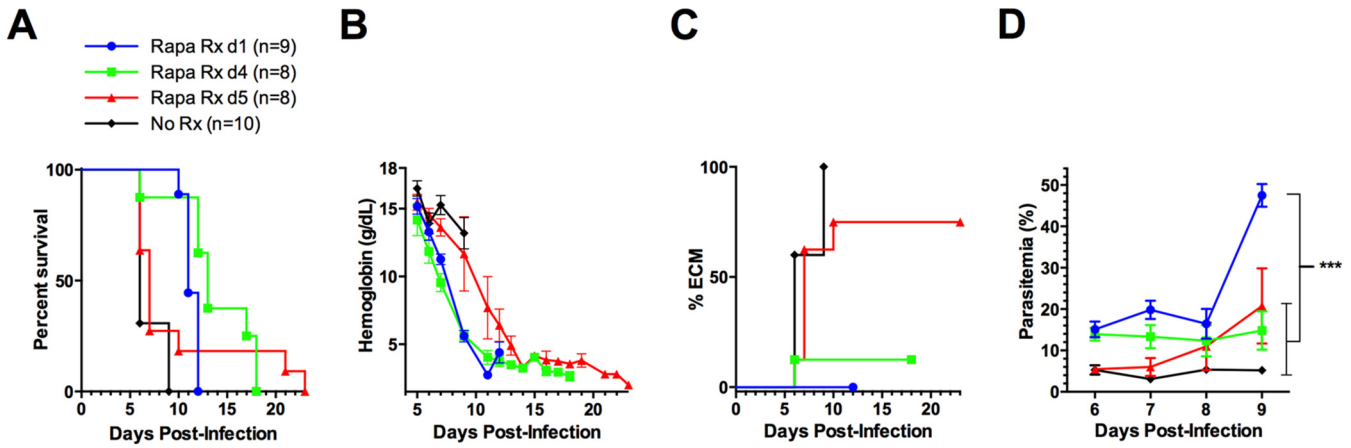

FIG 1 Treatment of mice with rapamycin prevents experimental cerebral malaria (ECM). Mice were infected with *Plasmodium berghei* ANKA (*Pb*A) by intraperitoneal injection of infected red blood cells (iRBCs) and treated with rapamycin (Rapa Rx) (1.0 mg/kg) or a control solution (no Rx) beginning on day 1 (d1), 4 (d4), or 5 (d5) postinfection (p.i.). The mice were monitored daily and scored for clinical neurological symptoms, and hemoglobin levels and parasitemias in peripheral blood were measured. (A) Percentage of mice in each group that survived with time after infection. (B) Hemoglobin levels measured in peripheral blood are given with time after infection. (C) The percentage of mice in each group that developed ECM defined as a clinical score above 6 with a hemoglobin level above 6 g/dl. (D) Peripheral blood parasitemias are given with time after infection. The results from one experiment representative of three independent experiments are shown. In two of the experiments, each experimental group had 8 to 10 mice; in the third experiment, each group had 5 mice. The parasitemia of mice treated with rapamycin (Rapa Rx) on day 1 was significantly higher than those of mice treated with Rapa Rx on day 4 or 5 and of control mice (no Rx) on 9 days p.i. Values that are statistically significantly different ($P \leq 0.0002$) are indicated by the bracket and three asterisks.

ginning rapamycin treatment on day 5 p.i. was considerably less effective, blocking ECM in only 20% of mice (Fig. 1A). Untreated mice died by day 9 with blood hemoglobin levels well above 6 g/dl. In contrast, mice that began rapamycin treatment on either day 1 or 4 p.i. showed dramatic drops in hemoglobin levels by day 9 p.i., indicating severe anemia (Fig. 1B). Using the criteria for ECM of clinical scores above 6 in severity and hemoglobin levels above 6 g/dl, it was apparent that all untreated mice and 80% of mice treated with rapamycin beginning on day 5 p.i. died of ECM (Fig. 1C), whereas all mice treated with rapamycin on day 1 p.i. and 90% of mice treated on day 4 p.i. were protected from ECM (Fig. 1C). Even though mice treated on day 1 or 4 p.i. were nearly equally protected from ECM, the mice treated with rapamycin beginning on day 1 p.i. died somewhat earlier than mice treated beginning on day 4 p.i. (Fig. 1A). Measurements of peripheral parasitemia showed that parasitemias in mice treated with rapamycin beginning on day 1 p.i. were significantly higher than mice treated with rapamycin beginning on day 4 or 5 p.i. and untreated mice (Fig. 1D). Thus, rapamycin treatment beginning on day 1 blocked the development of ECM despite enhancing peripheral parasite growth.

The presentation of neurological symptoms in mice with ECM is accompanied by focal hemorrhaging and disruption of the blood-brain barrier (BBB) (13). We assessed the effect of rapamycin treatment on the integrity of the BBB by measuring the exclusion from brain tissue of Evans blue (EB), a dye that binds to serum albumin that leaks into the brain parenchyma with BBB dysfunction (28, 29). *Pb*A-infected mice were treated with rapamycin daily beginning on day 1 or 4 p.i. or with a vehicle control solution. Brains from mice infected with *P. berghei* NK65 (*Pb*NK65), a parasite highly related to *Pb*A but one that does not cause ECM and results in severe anemia (30, 31), served as a negative control. The *Pb*NK65-infected control mice showed no leakage of EB into the brain by visual inspection of the brains (Fig. 2A). In contrast, *Pb*A-infected, untreated mice showed severe leakage of EB into the brain both visually and as quantified by extracting EB from the brain. *Pb*A-infected mice treated with rapamycin daily beginning on day 1 or 4 p.i. showed with minimal EB leakage into the brain (Fig. 2A). In separate experiments, rapamycin treatment starting on day 5 p.i. did not prevent BBB dysfunction, and the brains from most of these mice contained similar amounts of EB compared to the brains of *Pb*A-infected mice treated with vehicle control (data not shown).

Uninfected mice and infected mice that were treated with rapamycin beginning on day 4 p.i. or left untreated were sacrificed on day 6 p.i., and their brains were removed for histological examination. Brain sections were stained with either hematoxylin and eosin (H&E) to detect petechial hemorrhages and sequestered iRBC hemozoin associated with ECM or with IgG-specific antibody to detect intraparenchymal IgG as a second measure of the loss of BBB integrity (32). The brains of infected, untreated mice showed petechial hemorrhages in H&E-stained brain sections (Fig. 2B). Quantification of hemorrhages showed greater hemorrhaging in the brains of *Pb*A-infected, untreated mice (an average of 7 per brain section) compared to *Pb*A-infected, rapamycin-treated mice (an average of 2 per section) (Fig. 2C). The brains of untreated, *Pb*A-infected mice showed strong intraparenchymal staining for IgG, whereas the brains of mice treated with rapamycin beginning on day 4 p.i. resembled the brains of uninfected mice with no detectable intraparenchymal staining for IgG (Fig. 2B), which is consistent with results using EB exclusion as a marker for BBB integrity. iRBCs, identified by the presence of the parasite-produced hemozoin, were frequently observed in *Pb*A-infected, untreated mice in H&E-stained brain sections along the venular endothelium (Fig. 2B) but only rarely observed in the brain vasculature of *Pb*A-infected mice that were treated with rapamycin daily beginning on day 4 p.i. The parasite loads in the brains of saline-perfused mice on day 6 p.i. were quantified by quantitative PCR (qPCR) of 18S rRNA (Fig. 2D). We observed a 4-fold decrease in parasite 18S rRNA in the brains of *Pb*A-infected

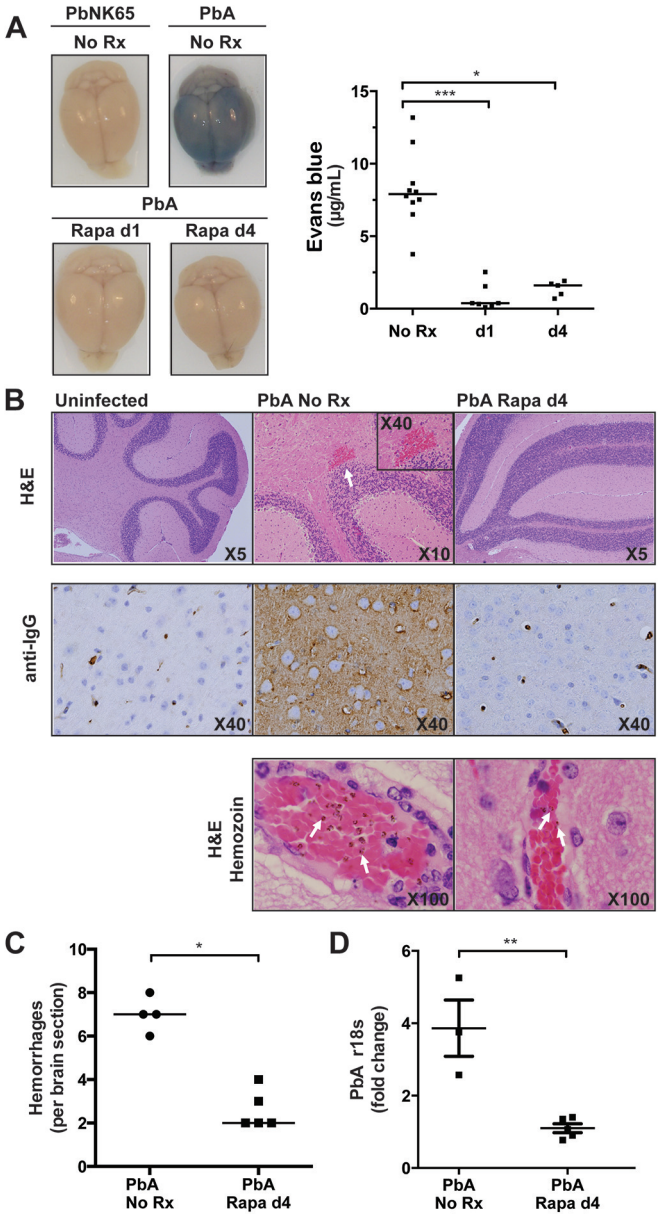

FIG 2 Rapamycin treatment prevents BBB dysfunction, brain hemorrhages, and accumulation of iRBCs in the brains of *Pb*A-infected mice. Mice were infected with either *Pb*A or *Pb*NK65 and left untreated (No Rx) or treated with rapamycin beginning on day 1 p.i. (Rapa d1) or day 4 p.i. (Rapa d4). (A) On day 6 p.i., mice were injected with Evans blue (EB), and 3 h later, the mice were anesthetized and transcardially perfused with cold PBS, and the brains were removed. Images of a representative brain from each group and the quantification of EB in all brains are shown. Data are from 5 to 10 mice in each group in two independent experiments. Each symbol represents the value for an individual mouse. The short black lines represent the median response for the group of mice. The median values that are statistically significantly different by Dunn's multiple comparisons for Kruskal-Wallis test are indicated by the brackets and asterisks as follows: *, $P = 0.0371$; ***, $P = 0.0003$. (B) Alternatively, on day 6 p.i., the brains of uninfected mice or of *Pb*A-infected mice that were treated with rapamycin beginning on day 4 p.i. or left untreated were removed for histological examination. (Top) Representative brain sections stained with H&E with the white arrow indicating a brain hemorrhage and an inset showing a higher-power (×40) image of the hemorrhage. (Middle) Representative sections stained with IgG-specific Ab to detect leakage of IgG into the brain. (Bottom) Representative H&E-stained brain sections in which iRBCs were detected by the presence of parasite-produced hemozoin. Images shown are representative of the images for mice (two to four mice in each group) in two independent experiments. (C) Quantification of hemorrhages on day 6 p.i. in the brains of *Pb*A-infected mice left untreated or treated with rapamycin beginning on day 4 p.i. Each symbol represents the number of hemorrhages for an individual mouse. The short black lines represent the median number of hemorrhages for the group of mice. The Mann-Whitney statistical test was used (*, $P = 0.0159$). (D) *Pb*A ribosomal 18S RNA was quantified in brains removed on day 6 p.i. from transcardially perfused mice that had been infected with *Pb*A and left untreated or treated with rapamycin on day 4 p.i. The results are expressed as a fold change compared to the values for three housekeeping genes, *hprt*, *gapdh*, and *ppia*. The lines and whiskers represent mean and standard deviation, respectively. The unpaired Student's *t* test was used (**, $P = 0.0034$). The results of one experiment of two independent experiments (3 to 5 mice in each group in each experiment) are shown.

(Continued)

Figure Legend Continued

mice treated daily with rapamycin beginning on day 4 p.i. compared to *Pb*A-infected, untreated mice despite equivalent levels of peripheral parasitemia in rapamycin-treated compared to untreated *Pb*A-infected mice (Fig. 1D). As expected, no qPCR amplification was detected in the brains of uninfected control mice with the same 18S ribosomal primers (data not shown). Taken together, these results show that administration of rapamycin as late as day 4 p.i. prevents the brain pathology associated with ECM, including breakdown of the BBB, brain hemorrhaging, and accumulation of iRBCs in the brain.

Rapamycin results in increased production of proinflammatory cytokines and chemokines. Because ECM is accompanied by the production of proinflammatory cytokines and chemokines, we determined the effects of rapamycin treatment on the serum levels of several inflammatory cytokines and chemokines, including interleukin 6 (IL-6), IL-10, IL-12p70, macrophage inflammatory protein 1α (MIP-1α), macrophage chemoattractant 1 (MCP-1), RANTES (*r*egulated on *a*ctivation, *n*ormal *T* cell *e*xpressed and *s*ecreted), IFN-γ, TNF-α, IL-1β, chemokine (C-X-C motif) ligand 1 (CXCL1), thymus and activation-regulated chemokine (TARC), and T cell alpha chemokine (TCA) using a cytokine array. Mice were uninfected or infected with *Pb*A and left untreated or treated with rapamycin daily beginning on day 1 or 4 p.i. All mice were sacrificed on day 6 p.i., and sera were collected. The sera of *Pb*A-infected, untreated mice had elevated levels of the proinflammatory molecules TCA, MIP-1α, CXCL1, MCP-1, RANTES, and IL-6 compared to uninfected mice, either treated with rapamycin or not treated with rapamycin (Fig. 3). The levels of IL-10, an anti-inflammatory cytokine often produced in response to inflammation (33), was also increased in *Pb*A-infected, untreated mice as compared to uninfected controls. Remarkably, daily rapamycin treatment of *Pb*A-infected mice beginning on day 4 p.i. resulted in significant increases in the serum levels of TCA, IFN-γ, MIP-1α, CXCL1, MCP-1, RANTES, and IL-6 (Fig. 3) compared to those of *Pb*A-infected, untreated controls. The level of the anti-inflammatory cytokine IL-10, which was higher in *Pb*A-infected mice than in uninfected mice, remained elevated in infected mice treated with rapamycin. In mice in which daily rapamycin treatment was started on day 1 p.i., we observed significantly higher levels of CXCL1 and significantly reduced levels of IL-10 (see Fig. S1 in the supplemental material) relative to *Pb*A-infected, untreated controls. These findings provide evidence that rapamycin prevents ECM even though treatment augmented the *Pb*A-induced systemic proinflammatory response.

Rapamycin treatment reduced the accumulation of leukocytes in the brain. ECM is accompanied by leukocyte sequestra-

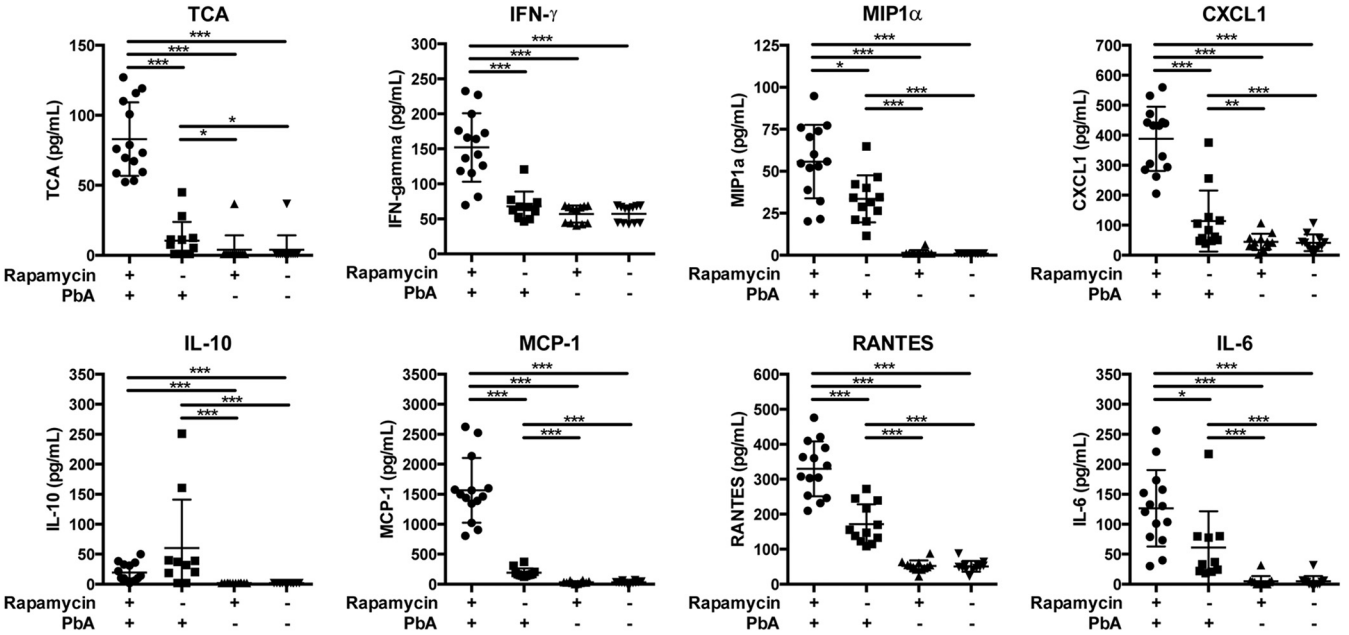

FIG 3 Daily treatment of *Pb*A-infected mice with rapamycin beginning on day 4 p.i. resulted in elevated levels of inflammatory cytokines and chemokines. Cytokine and chemokine levels were measured using a Q-Plex array mouse cytokine kit on day 6 p.i. in sera from uninfected mice or *Pb*A-infected mice left untreated (−) or treated with rapamycin (+) daily beginning on day 4 p.i. The levels of the following cytokines or chemokines are shown: TCA, IFN-γ, MIP-1a, CXCL1, IL-10, MCP-1, RANTES, and IL-6. Each experimental group contained 12 to 14 mice. The results from one experiment are shown. Values that are significantly different by Mann-Whitney tests are indicated by bars and asterisks as follows: *, $P < 0.05$; **, $P < 0.005$; ***, $P < 0.0005$.

tion in the brain, including $CD4^+$ and $CD8^+$ T cells, monocytes, neutrophils, and NK cells. We determined the number of total $CD4^+$ and $CD8^+$ T cells and the number of $CD44^+$ effector/memory T cells, neutrophils, and NK cells in the brains and spleens of uninfected mice and *Pb*A-infected mice that were either untreated or treated with rapamycin daily beginning on day 1, 4, or 5 p.i. All mice were terminally anesthetized on day 6 p.i. and transcardially perfused with phosphate-buffered saline (PBS). The brains and spleens were removed, processed, and analyzed by flow cytometry. The gating strategy used to identify total $CD4^+$ and $CD8^+$ T cells and effector/memory T cells, neutrophils, and NK cells is shown (see Fig. S2 in the supplemental material). We observed a large accumulation of $CD8^+$ T cells in the brains of *Pb*A-infected mice (1.0×10^5 cells per brain) (Fig. 4A) and a somewhat smaller accumulation of $CD4^+$ T cells (3.0×10^4 cells per brain) (Fig. 4B) compared to uninfected mice. More than 80% of the $CD8^+$ T cells that accumulated in the brain were $CD44^+$ effector/memory T cells (Fig. 4C), and similarly, the majority of $CD4^+$ T cells that accumulated in the brain, more than 60%, were $CD44^+$ effector/memory T cells (Fig. 4D). Treatment of *Pb*A-infected mice with rapamycin beginning on day 1 p.i. resulted in a dramatic reduction in the accumulation of both $CD4^+$ T cells (an 88% reduction) and $CD8^+$ T cells (a 99% reduction) in the brain (Fig. 4A to D). Treatment with rapamycin beginning on day 4 p.i. also resulted in reduced numbers of $CD4^+$ and $CD8^+$ T cells in the brain, and although these reductions were not as great as those observed in mice treated with rapamycin daily beginning on day 1 p.i., mice treated on day 1 or day 4 p.i. were similarly protected from ECM (Fig. 1C). There were no significant differences in the numbers of $CD4^+$ or $CD8^+$ T cells in the brains of mice treated with rapamycin on day 5 p.i. compared to untreated *Pb*A-infected mice (Fig. 4A to D), which is consistent with the weak protection from ECM (20%) of mice treated with rapamycin on day 5 p.i. The effects of rapamycin on the expansion of $CD8^+$ and $CD4^+$ T cells in spleens were more modest than the effect on the accumulation of these cells in brains. The number of $CD8^+$ effector/memory T cells increased approximately 3-fold in the spleens of *Pb*A-infected mice as compared to uninfected mice. Rapamycin treatment inhibited this increase, with the most effective inhibition (67%) observed for mice treated with rapamycin beginning on day 1 p.i. (Fig. 4E). The number of $CD4^+$ effector/memory T cells increased approximately 2-fold in the spleens of *Pb*A-infected mice compared to uninfected mice, and rapamycin blocked this increase but only when treatment began on day 1 p.i. (Fig. 4F). Together these results suggest that rapamycin treatment functions to protect mice against ECM at least in part by blocking the expansion of effector/memory T cells in peripheral lymphoid tissues and their migration to the brain, resulting in greatly diminished numbers of T cells accumulating in the brains of infected mice. Compared to uninfected mice, the number of neutrophils dramatically increased (more than 100-fold) in the brains of *Pb*A-infected mice, and rapamycin treatment beginning on day 1 or day 4 p.i. blocked this increase significantly. The number of neutrophils in the spleen did not increase with *Pb*A infection, and rapamycin treatment resulted in increased numbers of neutrophils in the spleens of infected mice consistent with the ability of rapamycin to block neutrophil chemotaxis (34). The number of NK cells in the brains of *Pb*A-infected mice increased 2.5-fold with *Pb*A infection, but rapamycin treatment had no effect on this increase (data not shown).

Rapamycin treatment during *Pb*A infection induced marked transcriptional changes in the brain and spleen. To obtain a global view of how rapamycin treatment prevented cerebral disease in *Pb*A infections, we carried out DNA microarray analyses of

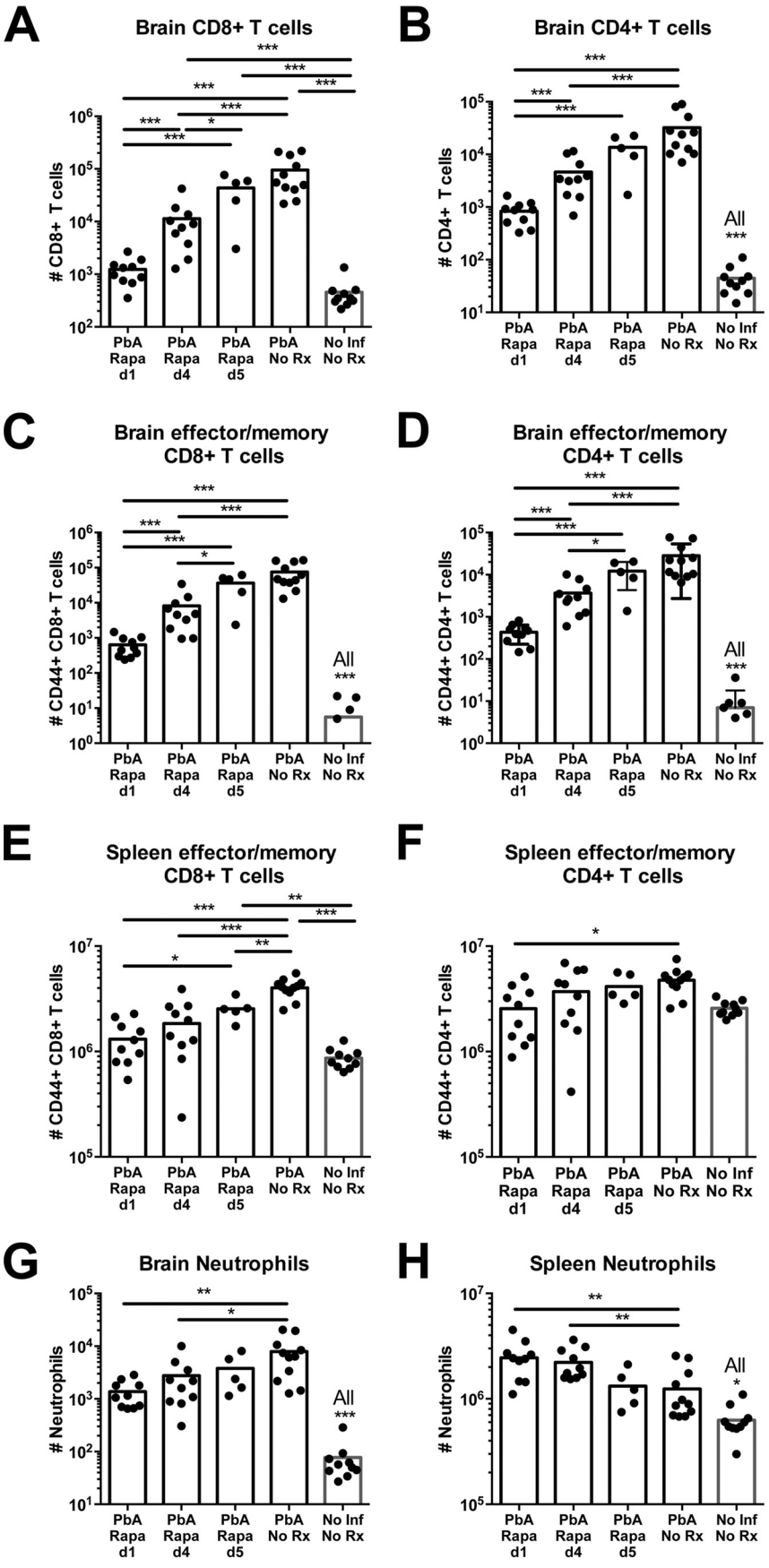
A
Brain CD8+ T cells
CD8+ T cells
B
Brain CD4+ T cells
CD4+ T cells
C
Brain effector/memory CD8+ T cells
CD44+ CD8+ T cells
D
Brain effector/memory CD4+ T cells
CD44+ CD4+ T cells
E
Spleen effector/memory CD8+ T cells
CD44+ CD8+ T cells
F
Spleen effector/memory CD4+ T cells
CD44+ CD4+ T cells
G
Brain Neutrophils
Neutrophils
H
Spleen Neutrophils
Neutrophils
All
PbA Rapa d1
PbA Rapa d4
PbA Rapa d5
PbA No Rx
No Inf No Rx

both brains and spleens at day 6 p.i. in mice that were treated with rapamycin beginning on day 1 p.i. or left untreated. Thus, four experimental groups were analyzed: uninfected mice, uninfected mice treated with rapamycin daily beginning on day 1 p.i., *Pb*A-infected mice, and *Pb*A-infected mice treated with rapamycin daily beginning on day 1 p.i. For the brain, the olfactory bulb, right cerebrum, and cerebellum were analyzed separately. The number of differentially expressed genes (DEGs) (cutoff criteria, absolute fold change of >1.5 and a false discovery rate [FDR] of <5%) for all comparisons are shown in Table S1 in the supplemental material (four mice in each group). Compared to uninfected mice, *Pb*A infection alone induced marked transcriptional changes in the olfactory bulb (1,107 DEGs), right cerebrum (509 DEGs), and cerebellum (589 DEGs). However, rapamycin treatment of *Pb*A-infected mice also induced substantial changes compared to untreated *Pb*A-infected mice, with 350 DEGs in the olfactory bulb, 215 DEGs in the right cerebrum, and 306 DEGs in the cerebellum. Notably, the vast majority of genes differentially expressed in *Pb*A-infected mice treated with rapamycin compared to untreated mice overlapped with genes differentially expressed in *Pb*A-infected versus uninfected mice (81% in the olfactory bulb, 78% in the right cerebrum, and 75% in the cerebellum) (Fig. 5A). Thus, rapamycin appears to abrogate cerebral disease in large part by altering the expression of the very same genes affected by *Pb*A infection. An even greater number of DEGs was observed in *Pb*A-infected spleens relative to uninfected spleens (2,560 DEGs) with a similarly high overlap between these DEGs and the 1,037 DEGs in rapamycin-treated, *Pb*A-infected mice compared to untreated *Pb*A-infected mice (see Fig. S3A in the supplemental material). It is important to note that rapamycin treatment of uninfected mice had little effect on the gene expression profiles relative to saline treatment (146 DEGs) and no effect on any part of the brains of uninfected mice (0 DEGs) (Table S1).

Differentially expressed gene sets from the *Pb*A-infected, rapamycin-treated mice versus *Pb*A-infected, untreated mice were further analyzed to determine which pathways were most highly affected by rapamycin treatment in the brain (Fig. 5B) and in the spleen (see Fig. S3B in the supplemental material). Canonical pathway enrichment analysis identified several affected pathways that were mutually overrepresented among the differentially expressed gene sets from all three brain tissues. These all involved immune cell pathways and included the following: granzyme A signaling; role of pattern recognition receptors; granulocyte/agranulocyte adhesion, diapedesis, and activation of interferon regulatory factors by cytosolic pattern recognition receptors (Fig. 5B). The finding that the pathways most highly affected by rapamycin treatment were associated with immune cell functions likely reflects the marked decrease observed in the numbers of immune cells, both T cells and neutrophils, in the brains of rapamycin-treated, *Pb*A-infected mice relative to untreated, *Pb*A-infected mice (Fig. 4A to D). In contrast, a number of immune pathways that are involved during *Pb*A infection are not affected by rapamycin treatment, suggesting that certain *Pb*A-affected pathways are distinct from the mechanism by which rapamycin blocks ECM. For example, expression of genes in the complement pathway are affected by *Pb*A infection compared to uninfected mice in all three parts of the brain, but rapamycin treatment had no effect on this pathway (Fig. 5B). The expression of subunits comprising the C1q complement complex was increased upon infection (for *C1qa*, 1.7-fold change and an FDR of 0.98% in the cerebrum, 1.6-fold change and an FDR of 3.0% in the olfactory bulb, and 1.7-fold change and an FDR of 1.3% in the cerebellum; for *C1qb*, 1.9-fold change and an FDR of 0.0024% in the cerebrum, 2.2-fold change and an FDR of <0.0001% in the olfactory bulb, and 2.7-fold change and an FDR of <0.0001% in the cerebellum) and unchanged by rapamycin treatment (not significant for *C1qa* and *C1qb* in all tissues). Although increased expression of C1q in the brain (35) and periphery (35, 36) has been suggested to play a role in pathogenesis in ECM, our results suggest that the development of ECM can be blocked despite such increases. Intriguingly, the antigen presentation pathway, which was significantly affected by *Pb*A infection in all three brain parts, was not altered in any case by rapamycin treatment (Fig. 5B). Consistent with this finding, expression of *Tap1*, which encodes an ATP-binding cassette peptide transporter that is critical in antigen processing for presentation on major histocompatibility class I molecules, was significantly upregulated in the brains of *Pb*A-infected mice versus uninfected mice (3.8-fold change and an FDR of <0.0001% in the cerebrum, 4.0-fold change and an FDR of <0.0001% in the olfactory bulb, and 3.6-fold change and an FDR of <0.0001% in the cerebellum), strongly implying increased antigen presentation in *Pb*A-infected mice. However, rapamycin treatment had no effect on these changes in *Tap1* expression. This finding suggests that although *Pb*A infection profoundly increases antigen presentation in the brain during infection, rapamycin-mediated protection against cerebral disease may not require the restoration of antigen presentation to uninfected levels.

Genes discordantly regulated in *Pb*A-infected mice treated with rapamycin are predicted to inhibit leukocyte recruitment and proliferation in brain tissue. Significant overlap among the DEGs in the *Pb*A-infected mice versus uninfected mice and the DEGs in the *Pb*A-infected, untreated mice versus *Pb*A-infected, rapamycin-treated mice suggests that rapamycin treatment may dampen specific subsets of genes that are induced by infection or vice versa. To identify changes in *Pb*A-induced gene expression that were abrogated or reversed by rapamycin treatment, DEGs for each part of the brain and spleen were filtered on those genes that showed a >1.5-fold change in expression in the comparison of *Pb*A-infected versus uninfected mice and a <−1.5-fold change in expression in the comparison of *Pb*A-infected, rapamycin-

FIG 4 Rapamycin treatment reduced the accumulation of leukocytes in the brains of *Pb*A-infected mice. Mice were infected with *Pb*A and treated with rapamycin beginning on day 1, 4, or 5 p.i. On day 6 p.i., mice were anesthetized and perfused with cold PBS, and brains and spleens were removed. Single-cell suspensions were prepared and analyzed by flow cytometry using the Abs and gating strategies described in the legend to Fig. S2 in the supplemental material. (A to H) The numbers of total $CD8^+$ cells in the brain (A), total $CD4^+$ T cells in the brain (B), effector/memory $CD8^+$ cells in the brain (C), effector/memory $CD4^+$ cells in the brain (D), $CD8^+$ effector/memory T cells in the spleen (E), $CD4^+$ effector/memory T cells in the spleen (F), neutrophils in the brain (G), and neutrophils in the spleen (H) are shown. The results shown are from 5 to 10 mice in each group combined from two of three independent experiments. Each black circle represents the value for an individual mouse. Error bars show the standard deviations. The statistical tests used were one-way ANOVA with Tukey posthoc tests for multiple comparisons computed on the $\log_{10}$-transformed data for each panel. Values that are significantly different are indicated by bars and asterisks as follows: *, $P < 0.05$; **, $P < 0.005$; ***, $P < 0.0005$.

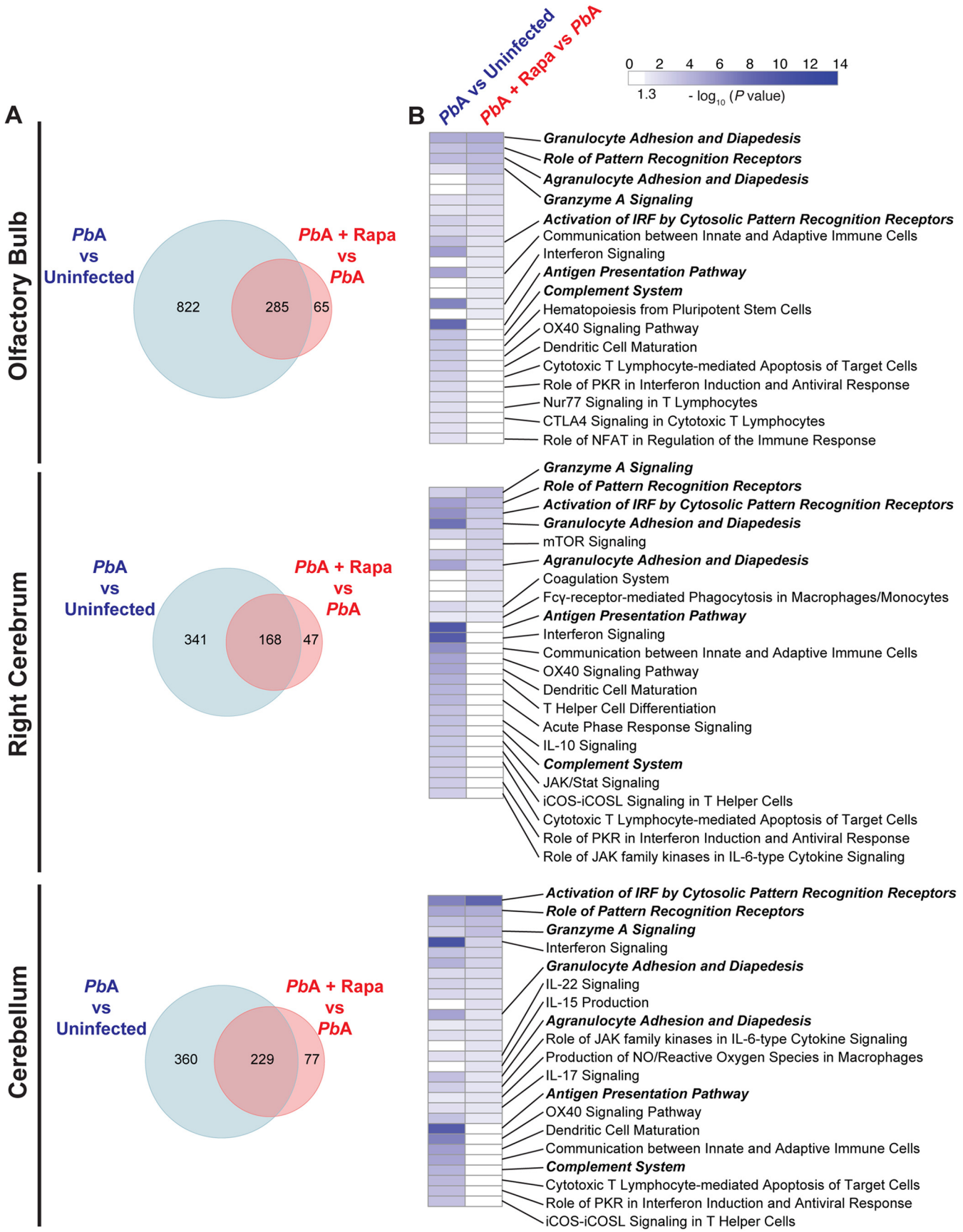
A
Olfactory Bulb
PbA vs Uninfected
PbA + Rapa vs PbA
822
285
65
Right Cerebrum
PbA vs Uninfected
PbA + Rapa vs PbA
341
168
47
Cerebellum
PbA vs Uninfected
PbA + Rapa vs PbA
360
229
77
B
PbA vs Uninfected
PbA + Rapa vs PbA
0 2 4 6 8 10 12 14
1.3
- log10 (P value)
Granulocyte Adhesion and Diapedesis
Role of Pattern Recognition Receptors
Agranulocyte Adhesion and Diapedesis
Granzyme A Signaling
Activation of IRF by Cytosolic Pattern Recognition Receptors
Communication between Innate and Adaptive Immune Cells
Interferon Signaling
Antigen Presentation Pathway
Complement System
Hematopoiesis from Pluripotent Stem Cells
OX40 Signaling Pathway
Dendritic Cell Maturation
Cytotoxic T Lymphocyte-mediated Apoptosis of Target Cells
Role of PKR in Interferon Induction and Antiviral Response
Nur77 Signaling in T Lymphocytes
CTLA4 Signaling in Cytotoxic T Lymphocytes
Role of NFAT in Regulation of the Immune Response
Granzyme A Signaling
Role of Pattern Recognition Receptors
Activation of IRF by Cytosolic Pattern Recognition Receptors
Granulocyte Adhesion and Diapedesis
mTOR Signaling
Agranulocyte Adhesion and Diapedesis
Coagulation System
Fcγ-receptor-mediated Phagocytosis in Macrophages/Monocytes
Antigen Presentation Pathway
Interferon Signaling
Communication between Innate and Adaptive Immune Cells
OX40 Signaling Pathway
Dendritic Cell Maturation
T Helper Cell Differentiation
Acute Phase Response Signaling
IL-10 Signaling
Complement System
JAK/Stat Signaling
iCOS-iCOSL Signaling in T Helper Cells
Cytotoxic T Lymphocyte-mediated Apoptosis of Target Cells
Role of PKR in Interferon Induction and Antiviral Response
Role of JAK family kinases in IL-6-type Cytokine Signaling
Activation of IRF by Cytosolic Pattern Recognition Receptors
Role of Pattern Recognition Receptors
Granzyme A Signaling
Interferon Signaling
Granulocyte Adhesion and Diapedesis
IL-22 Signaling
IL-15 Production
Agranulocyte Adhesion and Diapedesis
Role of JAK family kinases in IL-6-type Cytokine Signaling
Production of NO/Reactive Oxygen Species in Macrophages
IL-17 Signaling
Antigen Presentation Pathway
OX40 Signaling Pathway
Dendritic Cell Maturation
Communication between Innate and Adaptive Immune Cells
Complement System
Cytotoxic T Lymphocyte-mediated Apoptosis of Target Cells
Role of PKR in Interferon Induction and Antiviral Response
iCOS-iCOSL Signaling in T Helper Cells

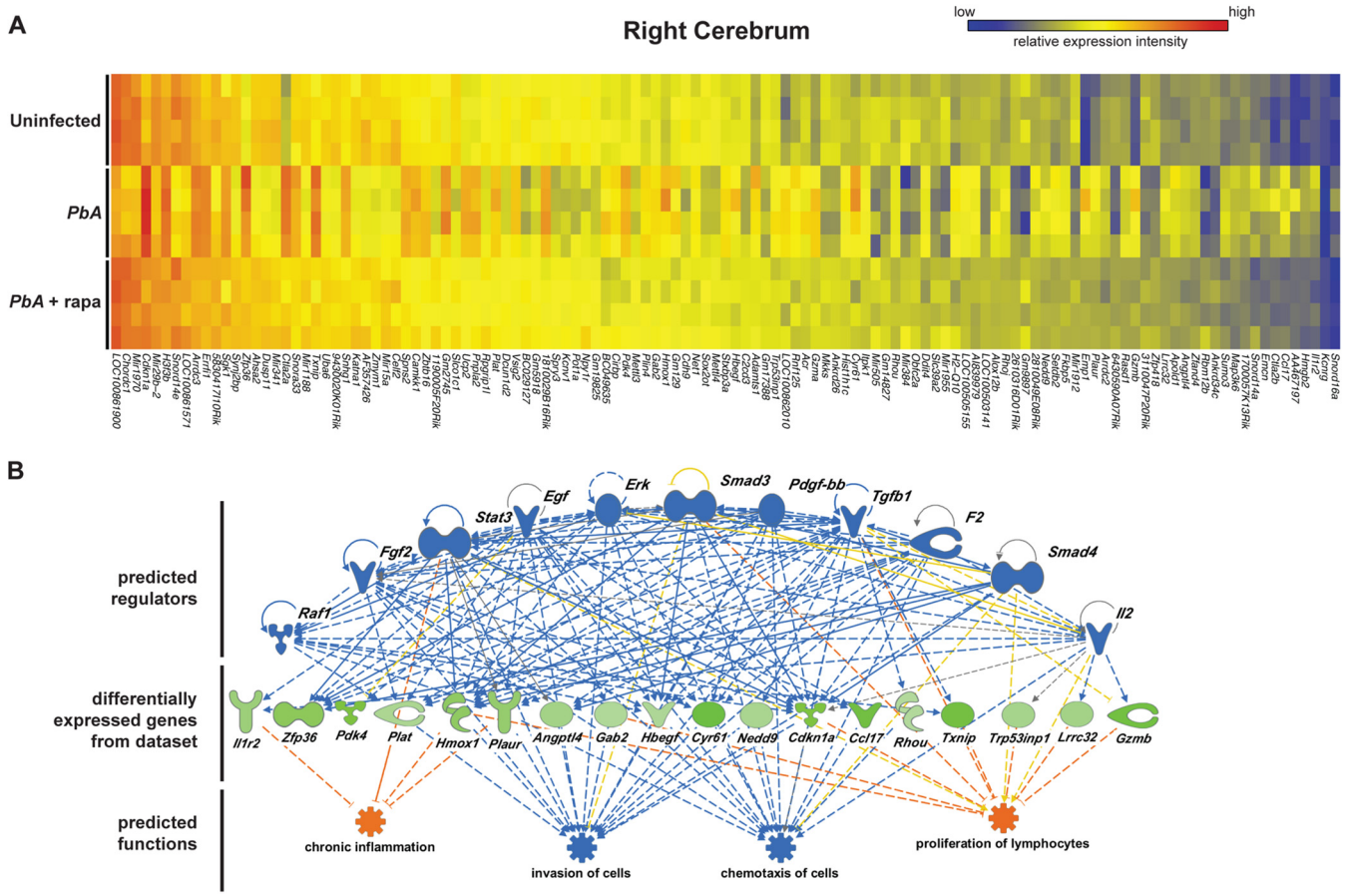

FIG 6 Rapamycin treatment reverses *Pb*A infection-induced transcriptional changes of genes involved in cellular chemotaxis, cellular invasion, and lymphocyte proliferation in the brains of *Pb*A-infected mice. (A) Heatmaps demonstrate differentially expressed genes identified by genome-wide DNA microarray analysis that have a change in expression of more than twofold for *Pb*A-infected mice relative to uninfected mice and a change of less than minus twofold for *Pb*A-infected, rapamycin-treated mice relative to untreated, *Pb*A-infected mice or vice versa, using a false discovery rate of <5% (three-way repeated measures ANOVA) for each comparison as the threshold for significance. Rows represent samples from each of the four individual mice. (B) Discordantly regulated genes determined using a less stringent fold change criteria (change in expression of greater than 1.5-fold for PbA-infected relative to uninfected mice and a change of less than −1.5-fold for *Pb*A-infected, rapamycin-treated mice relative to untreated, *Pb*A-infected mice or vice versa) were applied to Ingenuity Pathway Analysis (IPS) to determine the top regulator effect network in the right cerebrum. Top-tier molecules indicate predicted upstream regulators of downstream molecules. Middle-tier molecules are genes from the data set that are discordantly regulated with rapamycin treatment in *Pb*A-infected mice. Here, all genes were experimentally determined to be downregulated with rapamycin treatment. Bottom-tier "gears" denote predicted functions. Arrows denote activation pathways, whereas T-capped lines denote inhibitory pathways. Predicted inhibition (blue), predicted activation (orange), findings inconsistent with the state of the downstream molecule (yellow), and regulation that cannot be predicted (gray) are indicated.

treated versus *Pb*A-infected, untreated mice (or vice versa) using an FDR of <5% for each comparison as the threshold for significance. Figure 6A shows the expression intensities of the discordantly regulated genes in the right cerebrum for uninfected mice, *Pb*A-infected mice, and *Pb*A-infected, rapamycin-treated mice. Pathway enrichment analysis was applied to this filtered set of discordantly regulated genes to predict the regulator effect networks that are reversed or abrogated by rapamycin treatment during *Pb*A infection (Fig. 6B). This network analysis predicted inhibition of the following immunological functions with rapamycin treatment during *Pb*A infection: cellular invasion, cellular chemotaxis, lymphocyte proliferation, and chronic inflammation

FIG 5 Rapamycin treatment induces changes in granzyme signaling and cellular adhesion and diapedesis pathways in the brains of *Pb*A-infected mice as determined by genome-wide DNA microarray analysis. Mice were infected with *Pb*A or mock infected with saline and treated with either saline or rapamycin beginning on day 1 p.i. On day 6 p.i., all mice were anesthetized and perfused with ice-cold PBS, and RNA was isolated for transcriptional profiling by DNA microarray from three regions of the brain: olfactory bulb, right cerebrum, and cerebellum (four mice in each tissue for each condition). Differentially expressed genes (DEGs) with an absolute fold change of >1.5 (false discovery rate of <5%) were determined for the indicated comparisons by three-way repeated measures ANOVA. (A) Venn diagrams show the numbers of mutually exclusive and intersecting genes for each indicated comparison within each brain tissue type. (B) IPA canonical pathway enrichment analysis of the DEGs was used to compare the effect of *Pb*A infection alone (left column in each column pair) with the effect of rapamycin on *Pb*A infection (right column) for each brain tissue type. Columns were sorted by descending $-\log_{10} P$ value in the right column followed by the left column so that the most significantly enriched pathways are on top. Nonsignificant pathways ($P \geq 0.05$ by Fisher's exact test) are shown as white boxes. IRF, interferon regulatory factor; PKR, protein kinase R; NFAT, nuclear factor of activated T cells; JAK, Janus kinase; iCOS, inducible costimulator; iCOSL, iCOS ligand; NO, nitric oxide.

(Fig. 6B). Thus, rapamycin treatment is predicted to reverse the effect of *Pb*A infection by altering critical immune cell pathways, including trafficking to the brain, proliferation in the brain, and cerebral inflammation. A similar analysis of discordantly regulated genes predicted chronic inflammation to be inhibited in the olfactory bulb with rapamycin treatment. However, no other immunological functions were found among the top regulator effect networks in the cerebellum using the same analysis of discordantly regulated genes.

There are several genes of interest in the set of discordantly regulated genes (Fig. 6A) that provide insights into the mechanisms underlying rapamycin's effects. Expression of heme oxygenase 1 (HO-1; encoded by *Hmox1*) has been shown to be highly upregulated in *Pb*A-infected, ECM-resistant mouse strains and to be required for protection against ECM (37). Unexpectedly, *Hmox1* was among the discordantly regulated genes, demonstrating increased expression in *Pb*A-infected mice relative to uninfected mice (2.8-fold change and an FDR of 0.008% in the cerebrum; 6.9-fold change and an FDR of <0.0001% in the olfactory bulb) but decreased expression (−2.0-fold change and an FDR of 2.7% in the cerebrum; −2.3-fold change and an FDR of 0.27% in the olfactory bulb) in rapamycin-treated, *Pb*A-infected mice (Fig. 6A). This finding suggests that *Hmox1* may not be absolutely required for protection from ECM. $CD8^+$ T cells expressing granzyme B (encoded by *Gzmb*) have been demonstrated to be required for the development of ECM (15). Consistent with this, *Gzmb* expression significantly increased in the brains of *Pb*A-infected mice exhibiting signs of ECM (in the right cerebrum, 5.7-fold change and an FDR of <0.0001%; in the cerebellum, 6.2-fold change and an FDR of <0.0001%; in the olfactory bulb, 4.9-fold change and an FDR of <0.0001%), but it significantly decreased in ECM-protected, *Pb*A-infected mice treated with rapamycin at day 1 p.i. (in the right cerebrum, −2.8-fold change and an FDR of <0.0001%; in the cerebellum, −2.5-fold change and an FDR of 0.0001%; in the olfactory bulb, −1.8-fold change and an FDR of 0.077%), a result that could be explained in part by decreased $CD8^+$ T cell recruitment in the brain (Fig. 4A and C).

An upstream regulator analysis of differentially expressed genes was carried out for all comparisons (*Pb*A-infected mice versus uninfected mice and *Pb*A-infected, rapamycin-treated mice versus *Pb*A-infected mice). The results predicted genes involved in both type I and type II interferon responses (*Ifng*, *Irf7*, *Ifna2*, *Irf3*, *Stat1*, and *Infb1*) and proinflammatory genes (*Tnf*, *Il1b*, and *Il6*) as transcriptional activators in *Pb*A-infected mice relative to uninfected controls both in the brain (Fig. 7A to C) and in the spleen (see Fig. S3C in the supplemental material). Consistent with the results of the serum cytokine analyses (Fig. 3 and Fig. S1), treatment of *Pb*A-infected mice with rapamycin further increased activation of both interferon and proinflammatory pathways in the spleen (Fig. S3C). Notably, treatment of *Pb*A-infected mice with rapamycin increased activation of interferon response genes in the brain (*Irf7*, *Irf3*, *Ifna2*, *Ifnb1*, and *Ifng*), but not proinflammatory genes downstream of the interferons (*Tnf*, *Il1b*, and *Il6*) (defined as a Z score of >2 and $P < 0.01$) (Fig. 7A to C). This suggests that, in the brain, rapamycin-mediated augmentation of inflammatory responses during *PbA* infection may be limited to the innate, interferon-related response and truncated prior to the initiation of the downstream mediators of inflammation. In contrast, rapamycin-mediated augmentation of the inflammatory response in the spleen during *Pb*A infection involves both innate interferon-related responses as well as downstream mediators of inflammation.

Treatment with rapamycin increased parasitemia by modulating the adaptive immune response. The results presented thus far provide strong evidence that rapamycin treatment daily beginning on day 1 p.i. or as late as day 4 p.i. protects mice from the pathology of ECM. However, rapamycin treatment beginning at day 1 p.i. also resulted in an increase in peripheral parasitemia compared to untreated *Pb*A-infected mice (Fig. 1D), resulting in a drop in hemoglobin levels (Fig. 1B). The effect of rapamycin treatment on parasitemia appeared to be specific for the ECM-causing *Pb*A, as rapamycin treatment of mice infected with the closely related parasite *Pb*NK65 did not result in a rise in peripheral parasitemia (Fig. 8A). Rapamycin treatment had some effects on parasitemia in *Pb*NK65-infected mice, but the effects were small. Rapamycin treatment appeared to delay the rise in *Pb*NK65 parasitemia compared to untreated mice (Fig. 8A), perhaps consistent with the reported inhibitory effect of rapamycin on parasite growth *in vitro* (26). Rapamycin treatment resulted in hemoglobin levels that dropped somewhat more slowly during the course of infection in *Pb*NK65-infected, rapamycin-treated mice compared to untreated infected mice (Fig. 8B), and the rapamycin-treated mice survived longer (Fig. 8C). To determine whether rapamycin's effect on parasitemia was intrinsic to *Pb*A or was dependent on the host's immune response, recombination-activating gene product 1 (RAG-1)-deficient mice (RAG-1 [KO {knockout}]) that lack B and T cells were infected with *Pb*A and treated with rapamycin or a saline control. *Pb*A infection does not cause ECM in RAG-1 [KO] mice, because the functions of $CD8^+$ and $CD4^+$ T cells are required for ECM pathology. Thus, *Pb*A-infected RAG-1 [KO] mice survive longer than *Pb*A-infected C57BL/6 mice and ultimately die of severe anemia caused by hyperparasitemia. Rapamycin treatment did not cause an increase in parasitemia in RAG-1 [KO] mice compared to untreated, *Pb*A-infected RAG-1 [KO] mice (Fig. 8D), resulting in similar decreases in hemoglobin levels and survival in treated and untreated mice (Fig. 8E and F). Thus, rapamycin's effect on *Pb*A parasitemia does not appear to be due to a direct effect on *Pb*A growth *in vivo* but rather to an indirect effect on adaptive-immune-response-dependent mechanisms that control parasitemia.

For rapamycin treatment to be useful as an adjunctive therapy, it will be necessary to control the rapamycin-induced increase in parasitemia. To determine the feasibility of increasing survival following rapamycin treatment with antimalarials, *Pb*A-infected mice treated with rapamycin beginning on day 1 or day 4 p.i. were treated with three daily doses of artesunate beginning on day 7 p.i. when parasitemias rise rapidly in rapamycin-treated, *Pb*A-infected mice. Artesunate treatment reduced parasitemias, increased hemoglobin levels, and increased survival of *Pb*A-infected, rapamycin-treated mice compared to mice not given artesunate (Fig. 9A to C). Treatment of *Pb*A-infected mice with artesunate alone on day 7 p.i. was not feasible, as nearly all mice die by day 7 p.i. in the absence of rapamycin treatment. Thus, rapamycin treatment in conjunction with artesunate treatment results in a significant increase in survival of *Pb*A-infected mice.

DISCUSSION

HCM, a common form of severe malaria, imposes a heavy health burden in sub-Saharan Africa in childhood mortality and among survivors in long-term neurological deficits. At present, we have

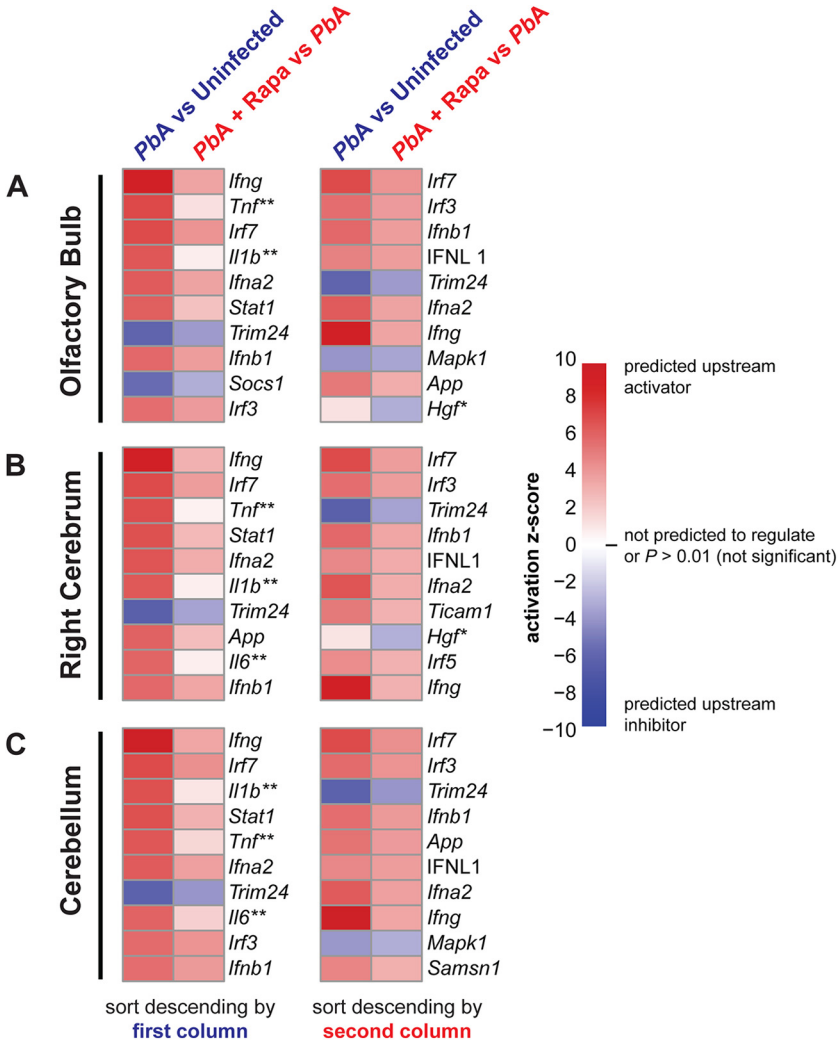

FIG 7 Upstream regulator analysis reveals tissue-specific augmentation of interferon responses in *Pb*A-infected mice treated with rapamycin. (A to C) Differentially expressed genes with an absolute fold change of >1.5 (false discovery rate of <5% by three-way repeated measures ANOVA) for each 2-way comparison were applied to IPA upstream regulator analysis to compare the effect of *Pb*A infection alone (left column in each column pair) and the effect of rapamycin on *Pb*A infection (right column) on predicted upstream transcriptional regulators in the olfactory bulb (A), right cerebrum (B), and cerebellum (C). Heatmaps demonstrate activation Z scores for predicted upstream activators (increasing red intensity) or predicted upstream inhibitors (increasing blue intensity) (overlap *P* value of <0.01 by Fisher's exact test). Column pairs are sorted by descending absolute Z scores on either the first comparison (left columns) or the second comparison (right columns). Only Z scores of less than −2 or more than 2 are considered significant. Therefore, a |Z score| of <2 is denoted by one asterisk for the first column and by two asterisks for the second column for each column pair.

no adjunctive therapies for HCM, and the development of such therapies would benefit greatly from a clearer understanding of the parasite and host mechanisms that underlie the pathology of HCM. Although our understanding of such mechanisms is far from complete, it seems likely that HCM pathology may have multiple causes with contributions from both the parasite and the host, particularly the host's immune response. HCM and ECM in mice share a number of features, including sequestration of iRBCs in the brain microvasculature, breakdown of the BBB, and elevated levels of proinflammatory cytokines (7, 13). It is well established that in ECM, $CD8^+$ T cells play a critical role in the pathogenesis of the infection (13), whereas in HCM, the functions of leukocytes observed in the brain vasculature (5, 12) remain uncharacterized.

Here we explored the effect of the mTOR inhibitor rapamycin on the progression of ECM in mice. Figure 10 depicts our current model for the effect of rapamycin on ECM. Rapamycin is an attractive candidate for therapy, as it has proven to be an effective means of suppressing immune responses (25). Moreover, rapamycin has been shown to inhibit the growth of *P. falciparum* in vitro through its binding to the parasite homolog of the mammalian FK506 binding protein (26). The effectiveness of rapamycin as an immunosuppressant is likely due to its ability to inhibit effector T cell differentiation and to inhibit effector T cell metabolism and thus function (25). Rapamycin treatment of mice during the first 3 days of infection was recently shown to increase survival in ECM with a concomitant decrease in the accumulation of $CD8^+$ and $CD4^+$ T cells in the brain (38). We observed that treatment with rapamycin as late as day 4 p.i. prevented ECM in mice. Treated mice showed none of the signs of pathology of ECM, including

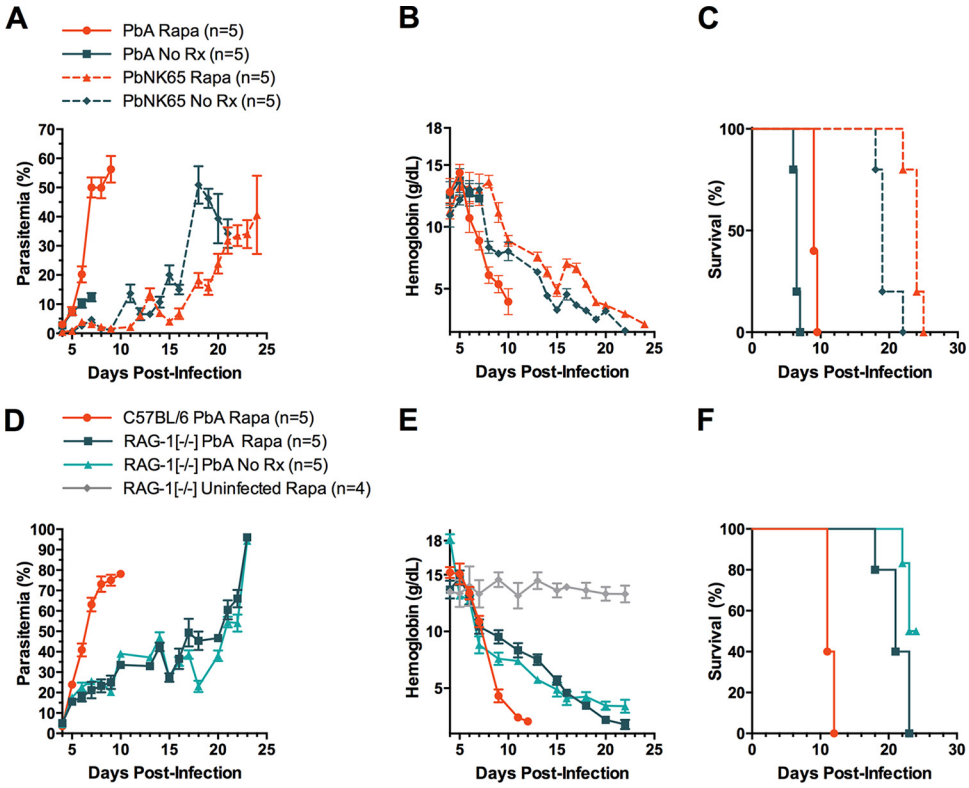

FIG 8 The rapid rise in parasitemia in rapamycin-treated mice is parasite strain specific and requires an intact adaptive immune system. Mice were infected with either *Pb*A or the closely related *Pb*NK65 strain and treated with rapamycin beginning day 1 p.i. or left untreated. (A to F) Peripheral blood parasitemias (A and D), blood hemoglobin levels (B and E), and survival with time after infection (C and F). C57BL/6 mice or RAG-1 [KO] mice were left uninfected or infected with *Pb*A and treated with rapamycin beginning on day 1 p.i. or left untreated. The data shown depict the results for 5 or 6 mice in each group from one experiment.

breakdown of the BBB, brain hemorrhaging, and neurological symptoms. Treatment with rapamycin resulted in a dramatic decrease in the number of $CD8^+$ T cells that accumulated in the brains of infected mice as well as the number of iRBCs in the brain vasculature. $CD8^+$ T cells have been established to play a critical role in ECM (13). Recent studies provided evidence that $CD8^+$ T cells engage parasite-derived peptides presented on MHC class I molecules on brain endothelium and in a perforin-dependent process damage the endothelium (20). On the basis of these observations, we propose that rapamycin blocks the differentiation of $CD8^+$ effector T cells in lymphoid organs and their migration to the brain, and in the absence of $CD8^+$ effector T cells in the brain, ECM does not develop.

Our comparison of the gene transcription profiles of unin-

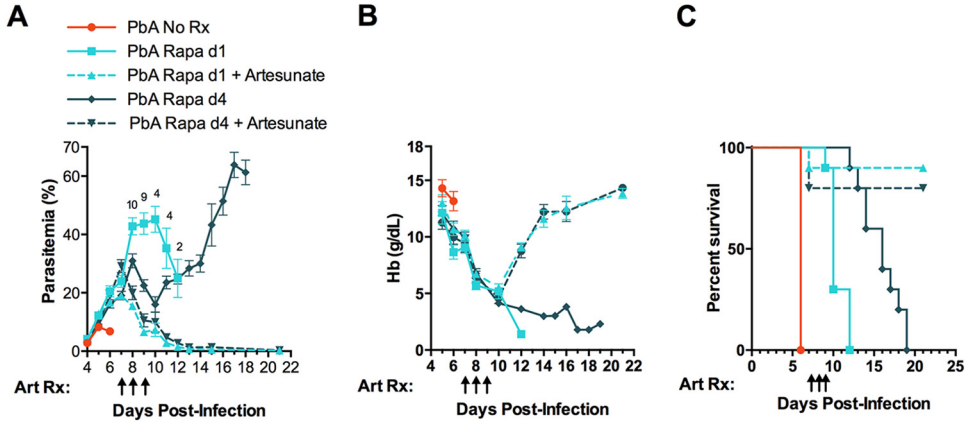

FIG 9 The rise in parasitemia in rapamycin-treated animals can be controlled by treatment with artesunate. Mice were infected with *Pb*A and left untreated or treated with rapamycin beginning on day 1 or day 4 p.i. with or without artesunate (Art) given on the days indicated by the black arrows. (A to C) Peripheral blood parasitemias (A), blood hemoglobin levels (B), and survival with time after infection (C). The data shown depict the results for 10 mice for each group from one experiment.

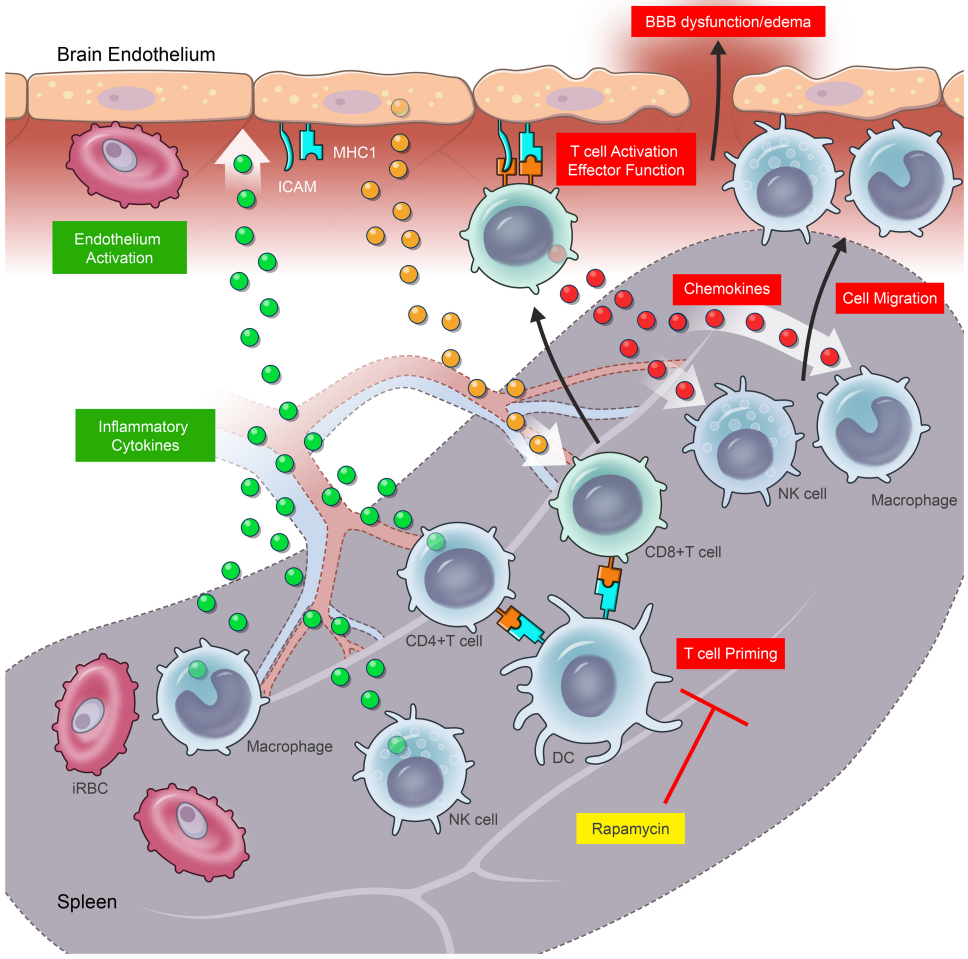

FIG 10 Model for the effect of rapamycin on ECM. As reviewed recently by Rénia and colleagues (46), ECM is initiated by the priming of $CD4^+$ and $CD8^+$ T cells in the spleen by dendritic cells (DC) that have processed and presented iRBC antigens. NK cells and monocytes in the spleen are also likely activated by iRBCs to secrete inflammatory cytokines. The brain endothelium is activated by interactions with iRBCs and in response to inflammatory cytokines. The activated endothelium produces chemokines that attract primed effector $CD8^+$ T cells from the spleen and cross presents parasite antigens on MHC class I molecules. $CD8^+$ T cells that have migrated to the brain are activated by engagement of MHC class I peptide complexes presented on the endothelium and release perforin and secrete chemokines that draw NK cells and macrophages to the brain. Together these immune cells further perturb the endothelium, resulting in loss of BBB function. Rapamycin functions to block T cell priming in the spleen. Consequently, the events downstream of T cell priming are blocked (shown in red). There is no migration of T cells, macrophages, or NK cells to the brain and no loss of BBB function. However, rapamycin would not be predicted to block activation of the endothelium by iRBCs or the production of inflammatory cytokine by non-T cells (shown in green). ICAM, intercellular adhesion molecule.

fected mice, *Pb*A-infected mice, and *Pb*A-infected, rapamycin-treated mice provided several novel insights into the molecular and cellular mechanisms underlying ECM. Perhaps most informative was the analysis of genes that were discordantly regulated in the brain; that is genes that were expressed at higher levels in *Pb*A-infected mice compared to uninfected mice but at lower levels in *Pb*A-infected, rapamycin-treated mice compared to untreated mice or vice versa. Analysis of the discordantly regulated genes showed that many such genes in the right cerebrum were involved in networks that regulate cellular chemotaxis and invasion and the proliferation of lymphocytes. Notably, *Pb*A-induced upregulation of *Gzmb*, which encodes granzyme B and plays an essential role in the development of ECM during *Pb*A infection in C57BL/6 mice (15), was significantly reversed with rapamycin treatment. These findings provide further evidence linking the recruitment of $CD8^+$ effector T cells to the brain with neuropathology, which may occur from endothelial damage by $CD8^+$ T cell-mediated cytotoxicity.

Remarkably, rapamycin treatment protected the brains of *Pb*A-infected mice despite inducing significant increases in inflammation both peripherally and in the brain. This conclusion was supported by our analyses of both cytokines and chemokines in peripheral blood and changes in gene transcription in the spleen and in the brain. The analyses of cytokines in serum provided evidence for large increases in inflammatory cytokines and a decrease in the anti-inflammatory cytokine IL-10. Comparisons of changes in gene transcription in the brains of *Pb*A-infected mice compared to uninfected mice and in *Pb*A-infected, rapamycin-treated mice showed that several inflammatory pathways were upregulated upon infection but even further upregulated upon rapamycin treatment. These findings were unexpected, since many studies have implicated inflammation as an integral aspect of CM pathogenesis. In fact, many features of severe malaria have been considered to be similar to those of sepsis (39), a condition of overwhelming inflammation. Intriguingly, our transcription analysis predicted that among the inflammatory genes,

only genes related to the interferon response would be activated in the brains of rapamycin-treated, *Pb*A-infected mice. Although downstream mediators of inflammation such as *Tnf*, *Il1b*, and *Il6* were predicted to be activated in the spleen after rapamycin treatment, similar activation of *Tnf*, *Il1b*, and *Il6* was not observed at any of the brain sites. These results suggest that the inflammatory cascade in the brains of *Pb*A-infected mice might be truncated or diminished locally by rapamycin treatment. In support of this, *Hmox1*, which is induced in response to oxidative stress and protects against ECM (37), was unexpectedly downregulated in the brains, but not the spleens, of *Pb*A-infected mice treated with rapamycin, suggesting that rapamycin protects from ECM by limiting oxidative stress events proximal to the induction of *Hmox1*. One could speculate that decreased recruitment of leukocytes to the brain conferred by rapamycin treatment reduces cytotoxic $CD8^+$ T cell-mediated end-organ damage and therefore limits inflammation and oxidative stress locally. Thus, limited end-organ inflammation could provide a possible explanation for why ECM was not observed in rapamycin-treated mice despite increased systemic inflammation. However, it remains to be seen whether this is a direct effect of rapamycin or simply a consequence of decreased leukocyte recruitment to the brain during *Pb*A infection. Rapamycin treatment may uncouple the *Pb*A-induced host inflammatory response, which may not in itself be necessary for the development of ECM, from the $CD8^+$ T cell-mediated response, which is required for ECM pathogenesis.

The results presented here also show that rapamycin treatment protects against ECM despite significantly increasing peripheral parasitemia. However, of perhaps greater importance, rapamycin treatment reduced parasite sequestration in the brains of infected mice which may be critical to ECM pathogenesis. In children with severe malaria, total parasite biomass, quantified by the serum concentration of *P. falciparum* histidine-rich protein 2 (*Pf*HRP2), was shown to be higher in fatal cases than in nonfatal cases despite both groups having equivalent peripheral parasitemias (40). Using the plasma concentrations of *Pf*HRP2 to quantify total, circulating, and sequestered parasite biomass, Cunnington et al. (41) recently showed that the sequestered biomass tended to be higher in children with HCM than in children with uncomplicated malaria, suggesting that sequestration of parasites in the brain, not total body parasitemia, may be critical to HCM pathogenesis (11). The mechanism by which rapamycin treatment enhanced parasite growth is also of potential interest. The observation that rapamycin treatment had no effect on parasite growth in RAG [KO] mice lacking an adaptive immune system suggests that rapamycin does not act directly on parasites but rather functions to relieve an immune mechanism that normally controls parasite growth. Understanding the nature of this mechanism may provide new targets for antimalarial drugs.

The demonstration that inhibiting mTOR-controlled metabolic pathways by treatment with rapamycin prevented the development of ECM opens up a new avenue toward developing adjunctive therapies for HCM by targeting the metabolism of the host immune cells. Recent studies suggest that several additional metabolic pathways are activated in T cells upon antigen recognition and are required for directing the resulting response (reviewed in reference 25). These pathways involve the transcription factors MYC, which drives cell growth and apoptosis and regulates glycolytic metabolism, and H1Fα, which regulates metabolism under hypoxic conditions as well as the serine/threonine kinase 5′ AMP-activated protein kinase (AMPK), which senses AMP/ATP ratios in cells to regulate cellular functions. Each of these pathways has critical and selective roles in defining T cell function and fate. Depending on the immune mechanisms at play in CM, inhibitors of these pathways may be more effective than rapamycin in controlling disease. For example, treatment with rapamycin inhibits the generation of effector $CD8^+$ T cells, requiring that rapamycin be administered before day 5 p.i., a time when the clinical symptoms of ECM are generally not apparent. It may be that inhibitors of metabolic pathways that are required for continued effector functions of T cells already present in the brains during CM could be delivered much later when neurological symptoms appear. Although best studied in T cells, metabolic pathways controlled by mTOR regulate diverse immune cell types that may play roles in HCM, including B cells, NK cells, neutrophils, and mast cells. Searches for inhibitors of cellular metabolism that block critical late immune cell function in CM may provide highly effective adjunctive therapies for HCM.

MATERIALS AND METHODS

Ethics statement. All experiments were approved by the National Institute of Allergy and Infectious Diseases Animal Care and Use Committee.

Animals and malaria infections. C57BL/6 and C57BL/6-[KO]RAG-1 female mice (7 to 10 weeks old) were obtained from the Jackson Laboratory. Mice were infected with either *Pb*A or *Pb*NK65 (New York line) by injecting 1×10^6 *Pb*A- or *Pb*NK65-iRBCs obtained from infected C57BL/6 mice intraperitoneally (i.p.). Hemoglobin levels in blood samples taken from the tail vein (<10 μl/day) were determined using a HemoCue Hb201+ (HemoCue AB, Angelholm, Sweden). Peripheral parasitemia was determined in blood either by Wright-Giemsa-stained whole-blood smears or by flow cytometry as described below. Infected mice were monitored for the progression of experimental cerebral malaria (ECM) using a 10-point clinical scoring system that rates mice as symptomless (a score of 0), to moribund (a score of 10), as previously described (42). According to our animal protocol, mice with a clinical score of 6 or greater and severely anemic mice with a hemoglobin level below 2.5 g/dl were euthanized.

Rapamycin and artesunate treatment. For rapamycin treatment, a stock solution of rapamycin (catalog no. R0395; Sigma Aldrich) was prepared by dissolving rapamycin in pure ethanol (25 mg/ml). For treatment of mice, which weighed approximately 20 g in these studies, the stock rapamycin solution was diluted in a solution of 5% polyethylene glycol 400 (Sigma), 4% ethanol, and 5% Tween 80 for a final concentration of rapamycin of 1 mg/ml. Mice were injected intraperitoneally with 1 mg/kg rapamycin every day starting on day 1, 4, or 5 p.i., unless otherwise noted. For artesunate treatment, 60 mg of artesunate (catalog no. A3731; Sigma) was dissolved in 1 ml of 5% sodium bicarbonate, to which 4 ml of 5% dextrose was added for a final concentration of 12 mg/ml. One hundred milligrams per kilogram was administered i.p. to mice on the specified days.

Flow cytometry of brain and spleen leukocytes. Mice were anesthetized with ketamine/xylazine 6 days p.i. and transcardially perfused with ice-cold PBS, and the brains and spleens were removed. The brains were dissected, minced, and digested with 1 mg/ml collagenase D for 30 min at 37°C. After the tissue was passed through 70-μm nylon mesh, homogenates were placed on a 90%−60%−40% discontinuous Percoll gradient and centrifuged for 18 min at $1{,}000 \times g$, and the cells at the 40%−60% interface containing mostly leukocytes were collected for analysis. The spleens were minced and forced through a 70-μm nylon mesh, and the cell suspension was incubated for 10 min in a solution of ammonium-chloride-potassium (ACK; Lonza) to lyse RBCs. The cells were washed and resuspended in RPMI 1640 with 10% heat-inactivated fetal bovine serum (FBS). The cells from both brain and spleen were stained in fluorescence-activated cell sorting (FACS) buffer (PBS plus 1% FBS). The

following fluorescent-dye-conjugated antibodies specific for the following cell surface markers were used for staining: brilliant violet 421-conjugated NK1.1 (BV421–NK1.1) (BioLegend), BV605–CD4 (BioLegend), BV785–CD8 (BioLegend), phycoerythrin-conjugated Ly6G (PE–Ly6G) (BD Pharmingen), phycoerythrin-and-Cy7-conjugated CD3 (PE-Cy7–CD3) (eBioscience), allophycocyanin-conjugated Ly6C (APC–Ly6C) (BD Pharmingen), Alexa Fluor 700-conjugated CD44 (AF700–CD44) (eBioscience), APC-Cy7–CD45.2 (BD Pharmingen), and LIVE/DEAD (Aqua; Invitrogen). Gating of subsets is depicted in Fig. S1 in the supplemental material. Cell acquisition data were obtained on a BD LSRII flow cytometer. Data were analyzed with FlowJo software (Tree Star Technologies).

Assessment of BBB integrity. Evans blue (20 mg/kg) was injected intravenously on day 6 p.i., and 3 h later, the mice were anesthetized and perfused, and the brains were removed and immediately frozen at −80°C for later processing. EB was quantified by a modified version of the previously described protocol (43). Briefly, EB was extracted from brains with one perfused brain per 2-ml skirted screw cap tube (Greiner). Seven hundred microliters of *N*,*N*-dimethylformamide (DMF) (catalog no. D4551; Sigma) was added with three silica beads (2.3 mm) (catalog no. 11079125z; Biospec) per tube and homogenized for 1 min at room temperature (Minibeadbeater-16 model 607; BioSpec Products). This homogenized solution was centrifuged at 16,000 × *g* for 20 min at 4°C. The supernatant was transferred to a separate tube and spun again at the same speed and temperature for 10 min. Two hundred microliters of this supernatant was then quantified in duplicate using a Varioskan Flash fluorometer (620-nm excitation; 695-nm emission; Thermo Scientific). For quantification, a standard curve was generated by using a uninfected perfused brain prepared in the same way and adding EB at a twofold dilution starting at 1 mg/ml to 1 μg/ml.

Quantification of peripheral blood parasitemia by flow cytometry. Parasitemia was determined by flow cytometry using a modified version of a previously described method (44). Briefly, blood (approximately 0.6 μl) was obtained from mouse tail veins, fixed with 0.025% aqueous glutaraldehyde solution, washed with 2 ml PBS, resuspended, and stained with the following: the DNA dye Hoechst 33342 (Sigma) (8 μM), the DNA and RNA dye dihydroethidium (diHEt) (10 μg/ml), an APC-conjugated antibody (Ab) specific for CD45.2 (BioLegend), a pan-C57BL/6 lymphocyte marker, and APC-Cy7-conjugated Ab specific for Ter119 (BD Pharmingen), an RBC marker. The cells were analyzed on a BD LSRII flow cytometer equipped with UV (325-nm), violet (407-nm), blue (488-nm), and red (633-nm) lasers. Data were analyzed using FlowJo software (Tree Star Technologies). iRBCs were CD45.2$^-$, Ter119$^+$, Hoechst positive, and diHEt$^+$. Overall parasitemia was calculated as the number of iRBCs/total number of RBCs.

Quantification of parasites localized in the brain. After anesthetization and intracardiac perfusion of mice as described above, the brains were removed, immediately frozen in liquid nitrogen, and pulverized, and RNA was extracted using a Qiagen RNeasy minikit according to the manufacturer's instructions. Genomic DNA was digested on a column using a RNase-free DNase set (Qiagen), and the elimination of genomic DNA was further confirmed using no reverse transcriptase (no-RT) controls. cDNA was generated using a iScript cDNA synthesis kit (Bio-Rad Laboratories). SYBR green PCR master mix (Bio-Rad) was used to determine the relative expression of parasite 18S rRNA and of three host housekeeping genes, *hprt*, *gapdh*, and *ppia*. The Pb-18S primers and primer sequences were 5′-AAGCATTAAATAAAGCGAATACATCCTTAC-3′ and 5′-GGAGATTGGTTTTGACGTTTATGTG-3′. The mouse *hprt*, *gapdh*, and *ppia* primer sequences were 5′-TGCTCGAGATGTGATGAAGG-3′ and 5′-TCCCCTGTTGACTGGTCATT-3′, 5′-GTGGAGTCATACTGGAACATGTAG-3′ and 5′-AATGGTGAAGGTCGGTGTG-3′, and 5′-TTCACCTTCCCAAAGACCAC-3′ and 5′-CAAACACAAACGGTTCCCAG-3′, respectively.

The geometric means of the threshold cycle (C_T) values of housekeeping genes were used as the baseline for comparing the ΔC_T value of 18S gene amplification. The changes in gene expression were calculated by comparing the ΔC_T values of experimental and control groups using the comparative C_T method ($2^{-\Delta\Delta CT}$).

Brain histology. Brain samples were fixed in 10% buffered formalin, embedded in paraffin, and sectioned. Sections were stained with hematoxylin and eosin (H&E) for ultrastructural examination and detection of hemorrhages and iRBC hemozoin. For detection of IgG, the slides were sequentially incubated in citrate for 20 min, 2% normal horse serum for 20 min, and biotinylated horse Ab specific for mouse IgG (Vector Labs, Burlingame, CA) for 30 min. Biotinylated horse Ab was detected using a biotin avidin peroxidase complex kit (Vector Labs). The slides were then examined by light microscopy with magnifications between ×5 and ×100, and the microscopic images were evaluated by two independent investigator in a blind manner (blind to the study design) as described previously (45). For quantitation of hemorrhages, 10 microscopic 40× power fields were examined, and the numbers of hemorrhages were counted and averaged.

Cytokine measurements. Blood samples were collected on day 6 p.i., and sera were stored at −80°C until analyzed for IL-6, IL-10, IL-12p70, MIP-1α, MCP-1, RANTES, IFN-γ, tumor necrosis factor alpha (TNF-α), IL-1β, CXCL1, TARC, and TCA using the Q-Plex array mouse cytokine kit (Quansys Biosciences) according to the manufacturer's instructions.

Microarray chip processing and data analysis. C57BL/6 mice were infected with *Pb*A or mock infected with saline vehicle and treated with either saline or rapamycin beginning on day 1 p.i. (4 conditions; 4 mice for each condition). On day 6 p.i., the mice were anesthetized and perfused with saline, and samples from 4 tissues (spleen, right cerebrum, cerebellum, and olfactory bulb; 64 samples total) were immediately frozen in liquid nitrogen. RNA was isolated. For each sample, labeled target was combined with 2× hybridization buffer, 3 nM B2 control oligonucleotide (catalog no. 900457; Affymetrix), 20× hybridization control stock (Affymetrix), and dimethyl sulfoxide (DMSO) making a final volume of 150 μl for the individual hybridizations to the Affymetrix GeneChip mouse gene 2.0 ST array containing the C57BL/6 mouse genome. The hybridization cocktail, including the components listed above, was denatured for 5 min at 99°C and then transferred to a 45°C heat block for an additional 5 min before transferring 130 μl of the cocktail onto the chip. The hybridization was carried out at a constant temperature of 45°C for approximately 40 h using an Affymetrix 640 hybridization oven. Upon completion of the hybridization step, each sample was removed from the chip and archived. Each chip was filled with approximately 160 μl of wash buffer A and then processed on the fluidics station 450. The reagents for the stain mixture consisted of 2× morpholineethanesulfonic acid (MES) stain buffer, 50 mg/ml of bovine serum albumin (BSA), 1 mg/ml of streptavidin phycoerythrin and water to make up a total volume of 600 μl for each stain. A holding buffer was added to make up a total volume of 800 μl for storage and scanning. Upon completion of the fluidics process, each sample was scanned using the Affymetrix GeneChip 3000 7Gplus scanner, and an expression console (Affymetrix version 1.3) was used to convert the data files to intensity (cel) files. The quality analysis was performed according to the "Quality Assessment of Exon and Gene Arrays" (Affymetrix revision 1.1). cel files representing individual samples were normalized using robust multiarray average (RMA) normalization followed by median normalization. Filtering was performed to remove any probe with mean $\log_2$ expression of all samples below 5.0 or $\log_2$ standard deviation of all samples below 1. Sample quality control was performed using principal component analysis (PCA) and sample-wise density plots in R. No outliers were identified in any of the aforementioned quality control methods used.

An empirical Bayes modified three-way repeated measure analysis of variance (ANOVA) was computed between the different treatment conditions using the limma package library in R to obtain false discovery rate (FDR)-adjusted *P* values and fold changes. The values for the probes were considered statistically significant if their FDR-adjusted *P* values were <0.05 and their absolute fold change was >1.5 except where otherwise

noted. Gene symbols, log fold change ratios, *P* values, and false discovery rates from the empirical Bayes ANOVA were imported into Ingenuity Pathway Analysis (IPA) (Qiagen) to determine pathway enrichment scores and perform upstream regulator and regulator effect analyses. Network diagrams were exported from IPA, and heatmaps were generated with the pheatmap package and gplots libraries in R.

Statistical analysis. Statistical analyses of nonmicroarray data were computed using the latest versions of GraphPad Prism 6. Most comparisons are unpaired Mann-Whitney tests with Bonferroni's adjustments for multiple comparisons applied when appropriate. Student's *t* test was computed for the qPCR data to allow for easier fold change calculation. One-way ANOVA with Tukey posthoc adjustments for multiple comparisons was used for the $\log_{10}$-transformed cell count data in Fig. 4. All survival curves are Kaplan-Meier curves with any log rank tests for any comparisons among curves.

SUPPLEMENTAL MATERIAL

Supplemental material for this article may be found at http://mbio.asm.org/lookup/suppl/doi:10.1128/mBio.00725-15/-/DCSupplemental.

Figure S1, PDF file, 1.6 MB.
Figure S2, PDF file, 1.1 MB.
Figure S3, PDF file, 2.2 MB.
Table S1, DOCX file, 0.01 MB.

ACKNOWLEDGMENTS

This study was supported by the Intramural Research Program of the National Institutes of Health, National Institute of Allergy and Infectious Diseases.

REFERENCES

1. **World Health Organization**. 2013. World malaria Report: 2013. World Health Organization, Geneva, Switzerland.
2. **Marsh K, Forster D, Waruiru C, Mwangi I, Winstanley M, Marsh V, Newton C, Winstanley P, Warn P, Peshu N, Pasvol G, Snow R**. 1995. Indicators of life-threatening malaria in African children. N Engl J Med **332:**1399–1404. http://dx.doi.org/10.1056/NEJM199505253322102.
3. **Dondorp AM, Fanello CI, Hendriksen IC, Gomes E, Seni A, Chhaganlal KD, Bojang K, Olaosebikan R, Anunobi N, Maitland K, Kivaya E, Agbenyega T, Nguah SB, Evans J, Gesase S, Kahabuka C, Mtove G, Nadjm B, Deen J, Mwanga-Amumpaire J, Nansumba M, Karema C, Umulisa N, Uwimana A, Mokuolu OA, Adedoyin OT, Johnson WB, Tshefu AK, Onyamboko MA, Sakulthaew T, Ngum WP, Silamut K, Stepniewska K, Woodrow CJ, Bethell D, Wills B, Oneko M, Peto TE, von Seidlein L, Day NP, White NJ, AQUAMAT group**. 2010. Artesunate versus quinine in the treatment of severe falciparum malaria in African children. (AQUAMAT): an open-label, randomised trial. Lancet **376:** 1647–1657. http://dx.doi.org/10.1016/S0140-6736(10)61924-1.
4. **Shikani HJ, Freeman BD, Lisanti MP, Weiss LM, Tanowitz HB, Desruisseaux MS**. 2012. Cerebral malaria: we have come a long way. Am J Pathol **181:**1484–1492. http://dx.doi.org/10.1016/j.ajpath.2012.08.010.
5. **Dorovini-Zis K, Schmidt K, Huynh H, Fu W, Whitten RO, Milner D, Kamiza S, Molyneux M, Taylor TE**. 2011. The neuropathology of fatal cerebral malaria in Malawian children. Am J Pathol **178:**2146–2158. http://dx.doi.org/10.1016/j.ajpath.2011.01.016.
6. **Milner DA, Jr, Whitten RO, Kamiza S, Carr R, Liomba G, Dzamalala C, Seydel KB, Molyneux ME, Taylor TE**. 2014. The systemic pathology of cerebral malaria in African children. Front Cell Infect Microbiol **4:**104. http://dx.doi.org/10.3389/fcimb.2014.00104.
7. **Grau GE, Craig AG**. 2012. Cerebral malaria pathogenesis: revisiting parasite and host contributions. Future Microbiol **7:**291–302. http://dx.doi.org/10.2217/fmb.11.155.
8. **MacCormick IJ, Beare NA, Taylor TE, Barrera V, White VA, Hiscott P, Molyneux ME, Dhillon B, Harding SP**. 2014. Cerebral malaria in children: using the retina to study the brain. Brain **137:**2119–2142. http://dx.doi.org/10.1093/brain/awu001.
9. **Turner GD, Ly YO, Nguyen TH, Tran TH, Nguyen HP, Bethell D, Wyllie S, Louwrier K, Fox SB, Gatter KC, Day NP, Tran TH, White NJ, Berendt AR**. 1998. Systemic endothelial activation occurs in both mild and severe malaria. Correlating dermal microvascular endothelial cell phenotype and soluble cell adhesion molecules with disease severity. Am J Pathol **152:**1477–1487.
10. **Schofield L, Grau GE**. 2005. Immunological processes in malaria pathogenesis. Nat Rev Immunol **5:**722–735. http://dx.doi.org/10.1038/nri1686.
11. **Cunnington AJ, Riley EM, Walther M**. 2013. Stuck in a rut? Reconsidering the role of parasite sequestration in severe malaria syndromes. Trends Parasitol **29:**585–592. http://dx.doi.org/10.1016/j.pt.2013.10.004.
12. **Grau GE, Mackenzie CD, Carr RA, Redard M, Pizzolato G, Allasia C, Cataldo C, Taylor TE, Molyneux ME**. 2003. Platelet accumulation in brain microvessels in fatal pediatric cerebral malaria. J Infect Dis **187:** 461–466. http://dx.doi.org/10.1086/367960.
13. **Rénia L, Howland SW, Claser C, Gruner A, Suwanarusk R, Teo T, Russell B, Ng LF**. 2012. Cerebral malaria: mysteries at the blood-brain barrier. Virulence **3:**193–201. http://dx.doi.org/10.4161/viru.19013.
14. **Craig AG, Grau GE, Janse C, Kazura JW, Milner D, Barnwell JW, Turner G, Langhorne J, participants of the Hinxton Retreat meeting on Animal Models for Research on Severe Malaria**. 2012. The role of animal models for research on severe malaria. PLoS Pathog **8:**e1002401. http://dx.doi.org/10.1371/journal.ppat.1002401.
15. **Haque A, Best SE, Unosson K, Amante FH, de Labastida F, Anstey NM, Karupiah G, Smyth MJ, Heath WR, Engwerda CR**. 2011. Granzyme B expression by CD8+ T cells is required for the development of experimental cerebral malaria. J Immunol **186:**6148–6156. http://dx.doi.org/10.4049/jimmunol.1003955.
16. **Baptista FG, Pamplona A, Pena AC, Mota MM, Pied S, Vigário AM**. 2010. Accumulation of Plasmodium berghei-infected red blood cells in the brain is crucial for the development of cerebral malaria in mice. Infect Immun **78:**4033–4039. http://dx.doi.org/10.1128/IAI.00079-10.
17. **McQuillan JA, Mitchell AJ, Ho YF, Combes V, Ball HJ, Golenser J, Grau GE, Hunt NH**. 2011. Coincident parasite and CD8 T cell sequestration is required for development of experimental cerebral malaria. Int J Parasitol **41:**155–163. http://dx.doi.org/10.1016/j.ijpara.2010.08.003.
18. **Yañez DM, Manning DD, Cooley AJ, Weidanz WP, van der Heyde HC**. 1996. Participation of lymphocyte subpopulations in the pathogenesis of experimental murine cerebral malaria. J Immunol **157:**1620–1624.
19. **Belnoue E, Kayibanda M, Vigario AM, Deschemin JC, van Rooijen N, Viguier M, Snounou G, Rénia L**. 2002. On the pathogenic role of brain-sequestered alphabeta CD8+ T cells in experimental cerebral malaria. J Immunol **169:**6369–6375. http://dx.doi.org/10.4049/jimmunol.169.11.6369.
20. **Howland SW, Poh CM, Gun SY, Claser C, Malleret B, Shastri N, Ginhoux F, Grotenbreg GM, Rénia L**. 2013. Brain microvessel cross-presentation is a hallmark of experimental cerebral malaria. EMBO Mol Med **5:**916–931. http://dx.doi.org/10.1002/emmm.201202273.
21. **Pai S, Qin J, Cavanagh L, Mitchell A, El-Assaad F, Jain R, Combes V, Hunt NH, Grau GE, Weninger W**. 2014. Real-time imaging reveals the dynamics of leukocyte behaviour during experimental cerebral malaria pathogenesis. PLoS Pathog **10:**e1004236. http://dx.doi.org/10.1371/journal.ppat.1004236.
22. **Schmidt KE, Schumak B, Specht S, Dubben B, Limmer A, Hoerauf A**. 2011. Induction of pro-inflammatory mediators in Plasmodium berghei infected BALB/c mice breaks blood-brain-barrier and leads to cerebral malaria in an IL-12 dependent manner. Microbes Infect **13:**828–836. http://dx.doi.org/10.1016/j.micinf.2011.04.006.
23. **Poh CM, Howland SW, Grotenbreg GM, Rénia L**. 2014. Damage to the blood-brain barrier during experimental cerebral malaria results from synergistic effects of $CD8^+$ T cells with different specificities. Infect Immun **82:**4854–4864. http://dx.doi.org/10.1128/IAI.02180-14.
24. **Powell JD, Pollizzi KN, Heikamp EB, Horton MR**. 2012. Regulation of immune responses by mTOR. Annu Rev Immunol **30:**39–68. http://dx.doi.org/10.1146/annurev-immunol-020711-075024.
25. **Pollizzi KN, Powell JD**. 2014. Integrating canonical and metabolic signalling programmes in the regulation of T cell responses. Nat Rev Immunol **14:**435–446. http://dx.doi.org/10.1038/nri3701.
26. **Bharatham N, Chang MW, Yoon HS**. 2011. Targeting FK506 binding proteins to fight malarial and bacterial infections: current advances and future perspectives. Curr Med Chem **18:**1874–1889. http://dx.doi.org/10.2174/092986711795496818.
27. **Hanson KK, Ressurreição AS, Buchholz K, Prudêncio M, Herman-Ornelas JD, Rebelo M, Beatty WL, Wirth DF, Hänscheid T, Moreira R, Marti M, Mota MM**. 2013. Torins are potent antimalarials that block replenishment of Plasmodium liver stage parasitophorous vacuole membrane proteins. Proc Natl Acad Sci U S A **110:**E2838–E2847. http://dx.doi.org/10.1073/pnas.1306097110.

28. **Yen LF, Wei VC, Kuo EY, Lai TW.** 2013. Distinct patterns of cerebral extravasation by Evans blue and sodium fluorescein in rats. PLoS One **8:**e68595. http://dx.doi.org/10.1371/journal.pone.0068595.
29. **Nag S.** 2003. Blood-brain barrier permeability using tracers and immunohistochemistry. Methods Mol Med **89:**133–144. http://dx.doi.org/10.1385/1-59259-419-0:133.
30. **Nacer A, Movila A, Baer K, Mikolajczak SA, Kappe SH, Frevert U.** 2012. Neuroimmunological blood brain barrier opening in experimental cerebral malaria. PLoS Pathog **8:**e1002982. http://dx.doi.org/10.1371/journal.ppat.1002982.
31. **Otto TD, Böhme U, Jackson AP, Hunt M, Franke-Fayard B, Hoeijmakers WA, Religa AA, Robertson L, Sanders M, Ogun SA, Cunningham D, Erhart A, Billker O, Khan SM, Stunnenberg HG, Langhorne J, Holder AA, Waters AP, Newbold CI, Pain A, Berriman M, Janse CJ.** 2014. A comprehensive evaluation of rodent malaria parasite genomes and gene expression. BMC Biol **12:**86. http://dx.doi.org/10.1186/s12915-014-0086-0.
32. **Richmon JD, Fukuda K, Maida N, Sato M, Bergeron M, Sharp FR, Panter SS, Noble LJ.** 1998. Induction of heme oxygenase-1 after hyperosmotic opening of the blood-brain barrier. Brain Res **780:**108–118. http://dx.doi.org/10.1016/S0006-8993(97)01314-0.
33. **Niikura M, Inoue S, Kobayashi F.** 2011. Role of interleukin-10 in malaria: focusing on coinfection with lethal and nonlethal murine malaria parasites. J Biomed Biotechnol **2011:**383962. http://dx.doi.org/10.1155/2011/383962.
34. **Liu L, Das S, Losert W, Parent CA.** 2010. mTORC2 regulates neutrophil chemotaxis in a cAMP- and RhoA-dependent fashion. Dev Cell **19:**845–857. http://dx.doi.org/10.1016/j.devcel.2010.11.004.
35. **Lackner P, Hametner C, Beer R, Burger C, Broessner G, Helbok R, Speth C, Schmutzhard E.** 2008. Complement factors C1q, C3 and C5 in brain and serum of mice with cerebral malaria. Malar J **7:**207. http://dx.doi.org/10.1186/1475-2875-7-207.
36. **Oakley MS, Anantharaman V, Venancio TM, Zheng H, Mahajan B, Majam V, McCutchan TF, Myers TG, Aravind L, Kumar S.** 2011. Molecular correlates of experimental cerebral malaria detectable in whole blood. Infect Immun **79:**1244–1253. http://dx.doi.org/10.1128/IAI.00964-10.
37. **Pamplona A, Ferreira A, Balla J, Jeney V, Balla G, Epiphanio S, Chora A, Rodrigues CD, Gregoire IP, Cunha-Rodrigues M, Portugal S, Soares MP, Mota MM.** 2007. Heme oxygenase-1 and carbon monoxide suppress the pathogenesis of experimental cerebral malaria. Nat Med **13:**703–710. http://dx.doi.org/10.1038/nm1586.
38. **Mejia P, Treviño-Villarreal JH, Hine C, Harputlugil E, Lang S, Calay E, Rogers R, Wirth D, Duraisingh MT, Mitchell JR.** 2015. Dietary restriction protects against experimental cerebral malaria via leptin modulation and T-cell mTORC1 suppression. Nat Commun **6:**6050. http://dx.doi.org/10.1038/ncomms7050.
39. **Langhorne J, Ndungu FM, Sponaas AM, Marsh K.** 2008. Immunity to malaria: more questions than answers. Nat Immunol **9:**725–732. http://dx.doi.org/10.1038/ni.f.205.
40. **Hendriksen IC, Mwanga-Amumpaire J, von Seidlein L, Mtove G, White LJ, Olaosebikan R, Lee SJ, Tshefu AK, Woodrow C, Amos B, Karema C, Saiwaew S, Maitland K, Gomes E, Pan-Ngum W, Gesase S, Silamut K, Reyburn H, Joseph S, Chotivanich K, Fanello CI, Day NP, White NJ, Dondorp AM.** 2012. Diagnosing severe falciparum malaria in parasitaemic African children: a prospective evaluation of plasma PfHRP2 measurement. PLoS Med **9:**e1001297. http://dx.doi.org/10.1371/journal.pmed.1001297.
41. **Cunnington AJ, Bretscher MT, Nogaro SI, Riley EM, Walther M.** 2013. Comparison of parasite sequestration in uncomplicated and severe childhood Plasmodium falciparum malaria. J Infect **67:**220–230. http://dx.doi.org/10.1016/j.jinf.2013.04.013.
42. **Waisberg M, Vickers BK, Yager SB, Lin CK, Pierce SK.** 2012. Testing in mice the hypothesis that melanin is protective in malaria infections. PLoS One **7:**e29493. http://dx.doi.org/10.1371/journal.pone.0029493.
43. **Kim JV, Kang SS, Dustin ML, McGavern DB.** 2009. Myelomonocytic cell recruitment causes fatal CNS vascular injury during acute viral meningitis. Nature **457:**191–195. http://dx.doi.org/10.1038/nature07591.
44. **Malleret B, Claser C, Ong AS, Suwanarusk R, Sriprawat K, Howland SW, Russell B, Nosten F, Rénia L.** 2011. A rapid and robust tri-color flow cytometry assay for monitoring malaria parasite development. Sci Rep **1:**118. http://dx.doi.org/10.1038/srep00118.
45. **Qi CF, Hori M, Coleman AE, Torrey TA, Taddesse-Heath L, Ye BH, Chattopadhyay SK, Hartley JW, Morse HC, III.** 2000. Genomic organisation and expression of BCL6 in murine B-cell lymphomas. Leuk Res **24:**719–732. http://dx.doi.org/10.1016/S0145-2126(00)00028-X.
46. **Howland SW, Claser C, Poh CM, Gun SY, Rénia L.** 2015. Pathogenic CD8 T cells in experimental cerebral malaria. Semin Immunopathol, in press. http://dx.doi.org/10.1007/s00281-015-0476-6.